Advances in veterinary investigative pathology techniques for porcine tissues

by

Jeana Lee Owens

B.S., Kansas State University, 2015

A THESIS

submitted in partial fulfillment of the requirements for the degree

MASTER OF SCIENCE

Department of Diagnostic Medicine/Pathobiology
College of Veterinary Medicine

KANSAS STATE UNIVERSITY
Manhattan, Kansas

2019

Approved by:
Co-Major professor
Anne Sally Davis

Approved by:
Co-Major professor
Ada Giselle Cino-Ozuna

Copyright

Abstract

Investigative pathology strives to link knowledge of disease presentation in the whole organism to the cellular and molecular changes caused by that disease. For this thesis I focused on understanding mechanisms of disease in animals that are relevant to disease presentation in humans. Development of novel diagnostics, medications, and treatments depend on animal studies. Due to their anatomical and physiological similarities to humans, pigs are a valuable experimental animal for researching diseases such as influenza. However, pigs are poorly characterized as regards their immune response to infectious diseases, and specifically in regard to influenza viruses. Therefore, to expand available knowledge on pigs as a model for human diseases, I focused on microscopic localization of immune cell markers as well as a marker for a host cell protease with a role in multiple diseases, including influenza.

My first objective was to validate a set of antibodies to visualize select porcine lymphocyte subsets and subtypes using immunohistochemistry (IHC) as part of a study to characterize naturally occurring severe combined immunodeficiency (SCID). SCID is a category of inherited disorders caused by various mutations that affect the adaptive immune system. Naturally occurring SCID has been found in pigs and once better characterized, SCID pigs have the potential to be a valuable biomedical research animal. Consequently, I developed IHC protocols for commercial antibodies, anti-CD3, anti-CD4, anti-Pax-5, including duplex protocols, CD3/CD4 and CD3/Pax-5 on formalin-fixed, paraffin-embedded (FFPE) porcine spleen. These IHC protocols can be used in future studies focused on characterization of lymphocyte presence and distribution in naturally occurring SCID in pigs as well as other studies where analysis of lymphocyte distribution in FFPE tissues is of value.

My second objective was to characterize the protein and mRNA expression of host cell protease, type II transmembrane protease, serine S1 member 2 (TMPRSS2 and *TMPRSS2*, respectively), in a diverse set of porcine tissues and compare these expression patterns to those reported in humans and mice. TMPRSS2 competently activates several respiratory viruses, in particular influenza A (IAV). Unlike mice, swine are naturally susceptible to human IAV strains and their responses to infections are clinically similar to those of humans. Consequently, there is a need to characterize the expression of this protease in the pig beyond the extant knowledge, which is limited to its expression in primary cells derived from the lower respiratory tract. IHC

and *in situ* hybridization (ISH) were used to analyze the distribution of TMPRSS2 and *TMPRSS2* in a wide variety of tissues. We found that porcine expression of this protease in the respiratory tract mirrored that in humans and that mice differ in their expression from both humans and pigs in the lower respiratory tract, specifically in their pneumocytes. Consequently, the pig may be a better experimental animal choice for studying the role of TMPRSS2 in human influenza and other respiratory viruses. Furthermore, the TMPRSS2 and *TMPRSS2* expression results for multiple other porcine tissue types should be of value to infectious disease and cancer research in other body systems.

Overall, the goal of this thesis was to expand available knowledge about pigs in support of their use as experimental animals in biomedical research. In the future, these two projects could come together because in multiple tissues TMPRSS2 was expressed in cells that are morphologically consistent with lymphocytes and it has been shown that lymphocytes play a role in IAV infection. When the necessary reagents for the experimental work under consideration are at hand, the pig should be considered as a suitable experimental animal because of the similarities in human and porcine physiological development and disease presentation.

Table of Contents

List of Figures

List of Tables

Acknowledgements

It would not have been possible to complete this thesis without help from a number of people around me, only some of whom it is possible to give mention here.

I would like to express my gratitude to my committee, Dr. A. Sally Davis, Dr. Ada Giselle Cino-Ozuna, and Dr. Bradley Njaa, for their guidance, patience, and precious time dedicated to completing this degree.

I would like to acknowledge the financial, academic, and technical support I received. This includes the Homeland Security Advanced Research Projects Agency of the Science and Technology Directorate of the United States Department of Homeland Security under contract number D15PC00276, National Institutes of Health under Award Number R24GVDM003822, University of Kansas Center for Biomedical Research Excellence in Protein Structure & Function (COBRE PSF), and the Department of Diagnostic Medicine and Pathobiology, College of Veterinary Medicine, Kansas State University.

I am forever grateful for the friends and family in my life that may not have understood my struggle but never left my side. Especially Courtney Weston, Lindsey Armbrust, Katie Schuck, Mya Masterson, Tony Kubina, the Rachels family, and many more. For providing love, support, encouragement, being willing to listen, and when all else failed a shoulder to cry on when it felt impossible to continue. A very special thank you to Nick, for being my partner, caring for me day in and day out, and above all never allowing me to give up on myself through the struggles and trials of this thesis.

Chapter 1 - Introduction

Investigative pathology strives to link knowledge of disease presentation in a whole organism to the cellular and molecular changes caused by that disease. In this thesis, I used veterinary investigative pathology techniques to understand mechanisms of disease in animals of relevance to human infectious disease research. Animals play a vital role in both animal and human medicine including the development of novel diagnostics, medications, and treatment methods. Numerous types of studies using animals in biomedical experiments have been conducted in the last few decades [1]. For example, researchers have used non-human primates, mice, ferrets, guinea pigs, hamsters, rats, and pigs to study influenza [2]. Pigs could potentially be a better biomedical research animal for influenza studies as well as for multiple other diseases due to their similarities to humans anatomically and in their physiological responses. However, pigs are still poorly characterized in their immune response to infectious diseases, and specifically there are gaps to be addressed as regards their use for influenza research [3]. Therefore, to expand available knowledge about pigs as a potential model for infectious disease research, I focused on the microscopic localization of immune cell markers as well as a marker for a host cell protease with a role in multiple viral diseases, including influenza.

My first objective was to optimize a set of antibodies to visualize multiple porcine lymphocyte subsets and subtypes for use in immunohistochemistry as part of a study of pigs with naturally occurring severe combined immunodeficiency (SCID). Decreased numbers of various leukocyte populations are a key factor in determining the type of SCID present [4]. Immunohistochemistry (IHC) is a technique that enables visualization of proteins within their histological context. This is achieved using specific antibodies and commercially available enzyme-based detection kits to visualize antigens that are markers for the protein of interest.

Typically, a secondary antibody binds to an unconjugated primary antibody-antigen complex in a tissue sample and after additional amplification and an enzymatic reaction with a chromogen, a color, the antigen of interest is visible using a brightfield microscope. For this first study, I developed multiple manual IHC protocols to visualize lymphoid subset markers for T lymphocytes and B lymphocytes. These protocols will be automated and used in the analysis of lymphoid tissues collected from SCID and normal pigs to further characterize the types of SCID present in support of their use in human medicine research.

My second objective was to characterize the protein and mRNA expression of host cell protease, type II transmembrane protease, serine S1 member 2 (TMPRSS2), in a diverse set of porcine tissues and compare these expression patterns to those reported in humans and mice. This protease has been identified as a key element in the activation of influenza virus and is a potential target for novel antiviral drugs [5, 6]. While some information on the expression of TMPRSS2 in human [7-9] and mouse tissues [10, 11] is available, its characterization in pig tissues is limited to primary cell cultures of porcine tracheal and bronchial epithelial cells [12]. First, I used IHC to determine TMPRSS2 protein expression in tissue, and where possible specific cell types, throughout the respiratory, gastrointestinal, and urogenital tract as well as other tissues. Then I used in situ hybridization (ISH) to examine mRNA (*TMPRSS2*) expression in the same tissues and analyzed how this correlated with the IHC findings. Finally, I compared porcine TMPRSS2 and *TMPRSS2* expression to human and murine expression. Porcine TMPRSS2 and *TMPRSS2* expression profiles for the porcine respiratory tract are valuable for future TMPRSS2 related influenza studies using pigs as the experimental animal. Additionally, these findings and those in the additional tissue types examined are of value to other research including infectious disease research into other respiratory and gastrointestinal viruses.

Chapter 2 - Immunohistochemistry Protocols for T and B Lymphocytes in Normal Pig Spleen for a Study of Severe Combined Immunodeficiency

Severe combined immunodeficiency (SCID) is a group of inherited disorders that can be caused by various mutations affecting the adaptive immune system. These disorders are grouped based on the mutation location and the deviations from the normal numbers of immune cells located in lymphoid tissues and circulating in blood [4]. The most common form of SCID results in a decrease or absence of T and B lymphocytes with normal levels of natural killer (NK) cells. T and B lymphocytes share a similar maturation process of certain gene segments of their cell surface receptors, including: the variable (V), diversity (D), joining (J), and constant (C) regions. During lymphocyte development, proper recombination of the V(D)J complex is critical for cells to fully mature and develop the diversity and specificity of their receptors. Specifically, during T lymphocyte antigen receptor (TCR) maturation, V(D)J recombination is responsible for the development of CD4 and CD8 markers on T helper lymphocytes and cytotoxic T lymphocytes respectively, as well as the B lymphocyte antigen receptor (BCR), which are all critical for adaptive immunity [13]. The absence of this recombination event results in a severely compromised immune system which increases susceptibility to common infectious diseases and shortens lifespan. In the late 1980s, SCID mice were established as an important biomedical research animal for the study of immunology and disease in humans [4]. However, physiological and cellular differences between humans and mice create many hurdles in the advancement of some research [14]. In recent years, pigs have emerged as an alternative animal model due to

their biological similarities to humans [15]. However, the absence of immunocompromised pig lines has slowed their use as an experimental animal in biomedical research.

Cino-Ozuna et al. 2011, discovered naturally occurring SCID in pigs that traced back to a line of Yorkshire pigs from Iowa State University (ISU) [16]. Researchers at ISU successfully farrowed additional SCID piglets, determined that this SCID was caused by two mutations in the *Artemis* gene, and collected initial data about their immune cell populations using flow cytometry [4]. Flow cytometry is a rapid diagnostic tool that can measure different traits of cells such as: cellular receptors, genomic content, size, and gene expression [15]. Interpretation of these traits together, enables identification of individual cell types or cell subpopulations of interest. By flow cytometry, the SCID pigs have a significant decrease in the number of circulating CD3+ T lymphocytes, and almost no CD4+ T lymphocytes, CD8+ T lymphocytes, or B lymphocytes in blood. This indicates that the *Artemis* mutations affect early lymphocyte development, likely interrupting V(D)J recombination [4]. Unfortunately, flow cytometry cannot provide information about the histological distribution of the cells. Consequently, the locations in lymphoid tissues impacted by the aforementioned lymphocyte subpopulation decreases are unknown. Such information is vital to understanding the type of SCID present in these pigs and the determination of their suitability for biomedical research.

Techniques are available to visualize the distribution of specific cell types within lymphoid tissues. Immunohistochemistry (IHC) is a research and diagnostic tool created from an overlap of chemistry, histology, and immunology. IHC is a proven technique that can accurately mark antigens present in specific cell types in tissue sections thereby enabling their visualization with histological context [17]. There are a variety of IHC methods available to detect an antigen's signal while minimizing non-specific background staining. Both direct and indirect

detection methods exist [17]. In a direct method, the antibody that binds the antigen of interest is directly conjugated to the reporter, a fluorophore or enzyme that reacts with a chromogen yielding a color deposit [16]. Indirect methods introduce one or more levels of amplification through use of molecules such as biotin, polymers, or tyramide. While they are generally more sensitive detection systems, they can be prone to generation of nonspecific background and often require additional blocking steps in their protocols. While IHC is a widely used technique, the optimization and validation of these assays can be difficult as each assay is always unique and heavily dependent on preanalytics [18].

While the number of available validated IHC assays is ever increasing, histology laboratories do not always have validated assays for all lymphocyte subsets of interest for all species of interest. In particular, there is a general lack of formalin-fixed, paraffin-embedded (FFPE) tissue IHC protocols for various mature porcine lymphocyte subsets [19]. Currently, the Kansas State Veterinary Diagnostic Laboratory (KSVDL) lacks validated FFPE porcine tissue IHC protocols for T lymphocyte subset markers CD4 and CD8α, as well as B lymphocyte nuclear marker Pax-5. In pigs as in other species, the spleen has a consistent distribution of lymphocytes. Its white pulp contains periarteriolar lymphoid sheaths (PALS), considered to be T lymphocyte rich areas, and the lymphoid follicles surrounding the PALS, B lymphocyte rich areas; while T lymphocytes predominate in the red pulp, where they are intermixed with other non-lymphocyte cells [20]. Hence, spleen is an ideal lymphoid tissue to use for lymphocyte marker IHC protocol development. Therefore, the aim of this project was to develop IHC protocols for T lymphocyte markers, CD3, CD4, and CD8 as well as a pan-B lymphocyte marker using commercially available antibodies and non-SCID pig spleen as the target tissue.

Materials and Methods

Tissues

Macroscopically normal spleen was collected from a euthanized adolescent male pig from an unrelated study at Kansas State University, College of Veterinary Medicine. The tissue, trimmed to 5 mm maximum thickness for optimal fixation, was placed in 10% neutral buffered formalin (NBF) for 48 hours. After fixation, the tissue was trimmed to roughly 3mm-thick sections, positioned in histologic cassettes, returned to NBF, and submitted to the KSVDL Histology Laboratory for routine processing and embedding into paraffin blocks. The tissues were sectioned at 4 μm onto positively charged slides. Hematoxylin and eosin stained slide review revealed microscopically normal spleen.

Table 1 Antibodies that successfully detected their target antigens

Marker	Antibody	Source	Antigen retrieval buffer	Detection system	Dilution	Antigen location
CD4	Mouse monoclonal anti-CD4 [clone 74-12-4]	Southern Biotech 4515-01	Sodium Citrate pH 6.0 (NaCit)	ImmPRESS- AP Reagent Anti-Mouse IgG (MP-5402)	1:50	Membrane
CD3	Rabbit polyclonal anti-CD3	Dako A0452	NaCit	ImmPRESS-HRP reagent kit peroxidase anti-rabbit Ig (MP-7401)	1:200	Membrane
Pax-5	Mouse monoclonal anti-Pax-5 [clone 24]	Sigma-Aldrich 312M-17	NaCit	ImmPRESS- HRP reagent kit peroxidase anti-mouse Ig (MP-7452)	Pre-diluted (ready to use)	Nucleus

Table 2. Antibodies that failed to detect their target antigens

Marker	Antibody	Source	Antigen location
CD4	Rabbit polyclonal anti-CD4	Abcam ab203034	Membrane
CD8	Mouse monoclonal anti-CD8 [clone 4SM15]	Thermo Fisher Scientific 14-0808-82	Membrane
CD8	Mouse monoclonal anti-CD8 [clone 76-2-11]	Novus Biologicals NBP1-28237	Membrane

Immunohistochemistry (IHC)

IHC protocols were developed to visualize lymphocyte markers in normal pig spleen. This included testing multiple antigen retrieval techniques, including: sodium citrate pH 6.0, Tris antigen unmasking solution pH 9.0 (H-3301; Vector Labs (VL) Burlingame, CA), DAKO target retrieval solution pH 6.1 (S1699; Agilent (Ag) Santa Clara, CA), and EDTA pH 9 (S236784-2; Ag). Multiple detection techniques were tried, including: Vectastain ABC (LS-J1010, LS-J1011; VL), Vectastain Elite ABC (PK-6101, PK-6102; VL), ImmPRESS-AP Reagent Anti-Mouse IgG (MP-5402; VL), ImmPRESS reagent kit peroxidase anti-rabbit Ig (MP-7401; VL), and ImmPRESS reagent kit peroxidase anti-mouse Ig (MP-7452; VL). The key components of the most successful protocols are detailed in **Table 1**. The antibodies listed in **Table 2** failed to produce appropriate signal with any combination of antigen retrieval method or detection technique.

In all cases, tissue sections were deparaffinized in xylenes and rehydrated through graded ethanols at 5 min intervals. Heat induced antigen retrieval (AR) was by vegetable steamer technique for 30 min. Washes performed between each step were with 1x tris buffered saline with 0.01% tween-20 (TBSt) unless otherwise specified. Endogenous Fc receptor labeling was

blocked using a 30 min incubation in Fc receptor block solution (NB309-30; INNOVEX biosciences; Richmond, CA). Use of primary antibody concentration matched isotype controls in all IHC runs enabled monitoring for nonspecific background due to the detection system.

Single Label IHC

CD3 and Pax-5

IHC protocols were developed to visualize both CD3 positive T lymphocytes and paired box protein 5 (Pax-5) positive B lymphocytes using a horseradish peroxidase-based (HRP) detection technique (**Table 1**). After antigen retrieval, endogenous peroxidase was blocked by incubating slides in 3% hydrogen peroxide diluted in DI water for 15 min at room temperature (RT). Nonspecific binding was blocked for mouse and rabbit raised primary antibodies with 20 min incubations of 2.5% normal horse serum block and 2.5% normal goat serum block, respectively. Anti-Pax-5 antibody (ready to use) and various concentrations (1:50 - 1:500) of anti-CD3 antibody (diluted in 1xTBS) were incubated on tissues for 1 hr at room temperature. Vector ImmPRESS anti-mouse and ImmPRESS anti-rabbit were incubated on the Pax-5 and CD3 (respectively) slides for 30 min then washed for 5 min. The markers were visualized by developing Vector ImmPACT VIP peroxidase substrate (SK-4605; VL) for 15 min or 3,3'-diaminobenzidine tetrahydrochloride (SK-4100; VL) for 2.5 min for Pax-5 and CD3 respectively. Tissues sections were washed in distilled water for 5 min before counterstaining with methyl green (H-3402; VL) at 60ºC for 5 min, rinsed in distilled water, and quickly dipped in acetone containing 0.05% (v/v) acetic acid 5 times. Tissue sections were express dehydrated using 30 sec intervals through graded alcohols, cleared in xylene, and mounted using Permount mounting medium (SP15-500; Thermo Fisher Scientific (TFS) Waltham, MA).

CD4

To evaluate CD4 positive T lymphocytes, an alkaline phosphatase detection technique was used (**Table 1**). After antigen retrieval, a 2.5% horse serum was placed on slides for 20 min to block nonspecific binding. After a brief rinse, anti-CD4 antibody diluted 1:50 in TBS was incubated on slides overnight at 4-6ºC. Slides were washed for 15 min and incubated with Vector ImmPRESS anti-mouse IgG for 30 min. ImmPACT Vector Red (SK-5105; VL) was made according to vendor guidelines with the addition of one drop of levamisole solution (SP-5000; VL) to block endogenous phosphatases and applied to the slides in the dark for 30 min at RT. The slides were washed with DI water for 5 min, quickly dipped 15 times in hematoxylin counterstain, and rinsed with tap water. Lastly, slides were express dehydrated using 30 sec intervals through graded alcohols, cleared in xylene and mounted using Permount mounting medium (SP15-500; TFS).

Dual Label IHC

CD3 and Pax-5

To evaluate the distribution of T and B lymphocytes in the same tissue section, a duplex IHC assay was developed. The slides were individually labeled with either anti-CD3 antibody or anti-Pax-5 antibody as detailed above. An additional two slides were run in parallel with both markers applied alternating which was applied first. One was first anti-CD3 visualized with DAB and second anti-Pax-5 visualized with ImmPACT VIP. The other was first anti-Pax-5 visualized with DAB and second anti-CD3 visualized with ImmPACT VIP. Slides were washed in distilled water for 5 min before counterstaining with methyl green at 60ºC for 5 min, rinsed in distilled water, and quickly dipped in acetone containing 0.05% (v/v) acetic acid 5 times. Slides were

express dehydrated using 30 sec intervals through graded alcohols, cleared in xylene, and mounted using Permount mounting medium.

CD3 and CD4

Despite attempts with the antibodies listed in **Table 2**, creation of a working CD8 IHC assay was not possible. Without a working anti-CD8 IHC assay, development of a CD4/CD8 duplex IHC protocol was impossible. Consequently, to visualize CD4 positive lymphocytes within the context of the overall T lymphocyte population a CD4 and CD3 duplex IHC assay was developed instead. The tissue sections were individually labeled with either anti-CD3 antibody or anti-CD4 antibody as detailed above. An additional two slides were run in parallel with both markers applied alternating which was applied first. One was first anti-CD3 visualized with DAB and second anti-CD4 visualized with Vector Red. The other was first anti-CD4 visualized with Vector Red and second anti-CD3 visualized with DAB. During the overnight incubation, all slides not incubating with anti-CD4 primary antibody were held in 1xTBS in the fridge. Slides were washed in distilled water for 5 min before counterstaining with methyl green at 60^{o}C for 5 min, rinsed in distilled water, and quickly dipped in acetone containing 0.05% (v/v) acetic acid 5 times. Slides were express dehydrated using 30 sec intervals through graded alcohols, cleared in xylene, and mounted using Permount mounting medium.

Results and Discussion

In this study, we developed immunohistochemistry protocols for lymphocyte subset markers Pax-5, CD3, and CD4 in FFPE pig spleen. Individual marker development was completed before optimizing markers in duplex, specifically CD3/CD4 and CD3/Pax-5. Macroscopically and microscopically normal spleen was selected for this work due to the

consistent and well documented distribution of T and B lymphocytes in this organ in many mammalian species, including pig [20, 21]. All three detection systems were free of non-specific background signal **(Figure 1)**.

Our Pax-5 IHC protocol successfully labeled B lymphocyte nuclei in normal porcine spleen. Pax-5, which encodes for a B lymphocyte specific transcription factor, is found in almost all stages of B lymphocyte maturation [22] making it an ideal marker to evaluate the total B lymphocyte population. Our most successful IHC technique used a polymer-based HRP detection and the VIP chromogen. We observed weak diffuse background staining of equivalent intensity throughout the connective tissue, capsule, and red pulp. However, stronger nuclear staining of varying intensity was readily observable above this background (**Figure 2A**). Lymphocytes labeled with anti-Pax-5 antibody were rarely present in the red pulp, and only occasionally seen in the marginal zone. Aggregates of positive cells were present near the outer periarteriolar lymphoid sheath (PALS) area, clearly forming lymphoid follicles. Rarely, Pax-5 positive cells were observed in the inner PALS area. We found Pax-5 positive cells in the marginal zone and lymphoid follicles consistent with the expected distribution of B lymphocytes in normal FFPE pig spleen [20].

Anti-CD3 antibody consistently labeled the cellular membranes of cells that were morphologically consistent with lymphocytes in the expected histological distribution for T lymphocytes in the spleen. The PALS and marginal zones of lymphoid follicles are T lymphocyte rich zones [23] . Additionally, T lymphocytes are occasionally found in the red pulp and primary lymphoid follicles in mouse spleen [24]. CD3 is exclusively expressed on T lymphocytes throughout all developmental stages [13] making it a logical marker for assessing the total T lymphocyte population. CD3 positive cells were scattered throughout the red pulp

increasing in their frequency immediately adjacent to white pulp (**Figure 2B**). Additionally, the majority of lymphocytes near the PALS were strongly positive. The marginal zone of the lymphoid follicles also contained CD3 positive lymphocytes; however, these were in lower numbers than those surrounding the PALS.

Creation of a T and B lymphocyte duplex assay wherein one marker labels the nuclear compartment (Pax-5) and the other is membranous (CD3) is particularly powerful as it provides high fidelity separation of signal and readily lends itself to quantification by digital image analysis. For the T and B lymphocyte dual label assay, application of the anti-CD3 antibody first and the anti-Pax-5 antibody second (CD3/Pax-5) worked best. In contrast, application of the anti-Pax-5 antibody first (Pax-5/CD3) was unsuitable because the Pax-5 signal was lost during application of anti-CD3 antibody. On sequential sections of the same FFPE tissue specimen, the CD3/Pax-5 assay labeled splenic lymphocytes equivalently to the respective CD3 (**Figure 2A**) and Pax-5 **(Figure 2B)** singleplex assays. The only observable difference was that lymphocytes positive for Pax-5 labeled less intensely in the dual IHC protocol **(Figure 2C)**, possibly due to light background created while labeling the CD3 positive cells.

It is generally accepted that most mature T lymphocytes express either CD4 or CD8 cell markers as a part of their T-cell antigen receptor (TCR) [24]. However, unlike other species, pigs have a small subset of T lymphocytes found outside the thymus that are both CD4 and CD8 positive [13, 25]. Given that the mutations in the *Artemis* gene of SCID pigs can affect the maturation process of T lymphocytes and significantly decrease the number of T helper cells and cytotoxic T cells [4], it is important to evaluate these subsets in SCID vs. normal pigs. Therefore, we attempted to develop IHC protocols for both anti-CD4 and anti-CD8 T lymphocyte antibodies.

Immunohistochemistry with rabbit polyclonal anti-CD4 antibody failed universally despite tests with a wide range of primary antibody dilutions (1:50 – 1:1000) and a variety of antigen retrieval methods and detection approaches. In contrast, mouse monoclonal anti-CD4 antibody [clone 74-12-4] produced a strong, specific cellular membrane signal with all antigen retrieval buffers when an alkaline phosphatase detection kit was used. Diffuse background staining was observed in the smooth muscle of the splenic trabeculae and the splenic capsule. Although the application of various antigen retrieval methods, blocking techniques, and adjustments of the primary antibody concentration all failed to completely resolve this background, it was reduced the most using the methods listed in **Table 1**. Above this background, cells morphologically consistent with lymphocytes had intense membranous signals. These CD4 positive cells also appeared in the same T lymphocyte rich regions of the spleen albeit in lower numbers than the CD3 positive cells (**Figure 3A-B**).

Unfortunately, our CD8 IHC development failed. Both antibodies, mouse monoclonal anti-CD8 [clone 4SM15 and clone 76-2-11] antibodies, produced no specific signal despite testing them with a variety of primary antibody concentrations, antigen retrieval methods and detection approaches. Consequently, we developed a dual IHC assay to evaluate the colocalization of CD3 and CD4 positive T lymphocytes. For this assay, application of the anti-CD3 antibody before the anti-CD4 antibody (CD3/CD4) worked best. In contrast, when the anti-CD4 antibody was applied before the anti-CD3 antibody (CD4/CD3) an intense diffuse background emerged causing loss of signal detection above the background. The distribution of cells positively labeled for CD4 mirrored that for CD3, but at a lower frequency (**Figure 3C**). As seen in previous characterizations of T lymphocyte subpopulations [23], our dual label T lymphocyte protocol appropriately identified differentiated T helper cells (CD4+) in spleen.

While we can evaluate CD4+ T lymphocytes in relation to CD3+ T lymphocytes, without a working CD8 marker we cannot rely on these results only to assess distribution of CD8+ T lymphocytes. Although a portion of CD3+/CD4- T lymphocytes could be CD8+, we do not know which CD4+ lymphocytes could also be CD8+.

In summary, we developed both singleplex and duplex IHC protocols for multiple lymphocyte markers that label different subsets of lymphocytes in porcine lymphoid tissue, specifically spleen. With further validation, these protocols can be used to characterize B and T lymphocyte distribution in a variety of porcine tissues including those in SCID pigs.

Acknowledgements

We thank Dr. Christopher K Tuggle and his laboratory group at Iowa State University.

Figure 1. Isotype antibody controls, pig spleen

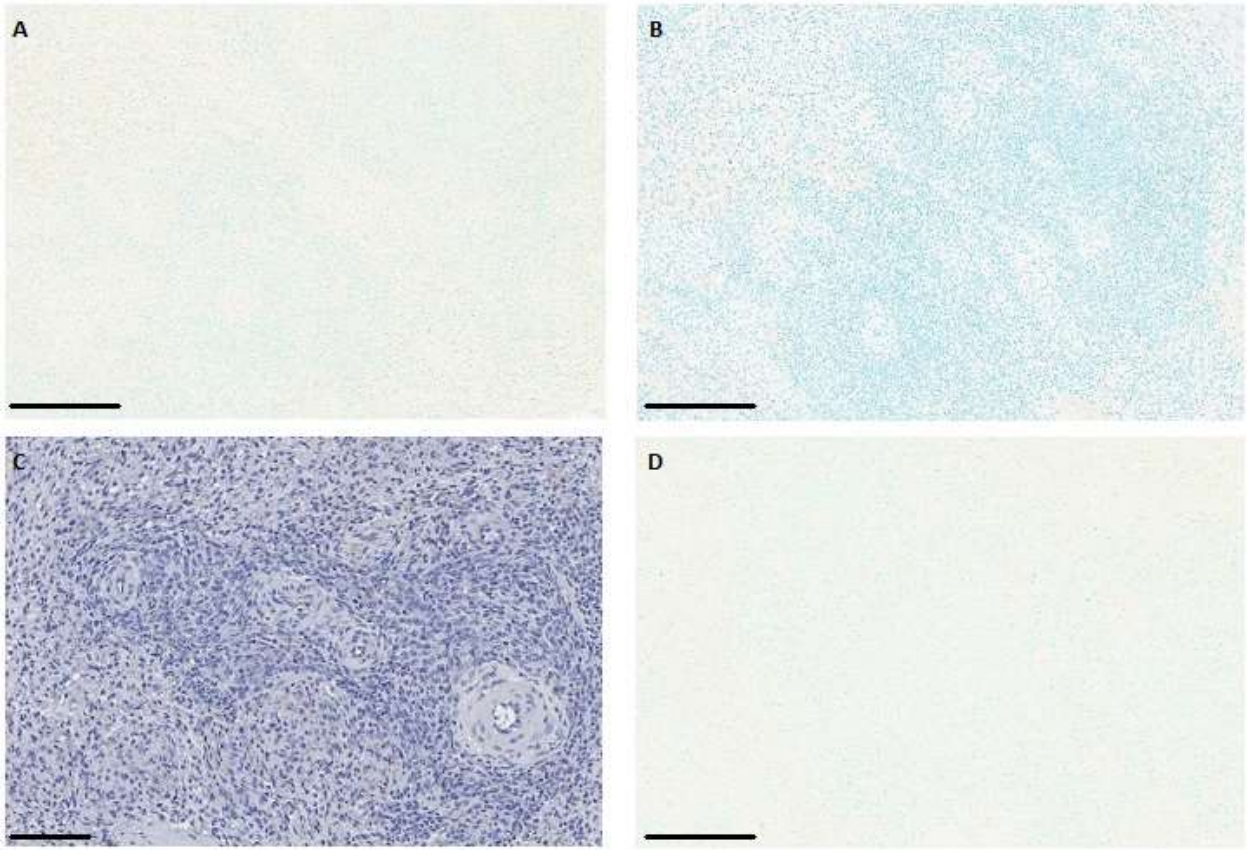

Application of mouse IgG1 or rabbit IgG isotype control antibodies instead of primary antibodies anti-CD3, anti-Pax-5, and anti CD4 in the final IHC protocols. No detectable signal was present (bar is 200 μm). **(A)** rabbit IgG isotype control, polymer-HRP detection system, DAB chromogen and methyl green counterstain (bar is 200 μm). **(B)** mouse IgG isotype control, polymer-HRP detection system, ImmPACT VIP chromogen and methyl green counterstain (bar is 200 μm). **(C)** mouse IgG isotype control, polymer-AP detection system, ImmPACT Vector Red chromogen, and hematoxylin counterstain (bar is 100 μm). **(D)** Both mouse IgG and rabbit IgG isotype controls, DAB and VIP chromogens respectively, and methyl green counterstain (bar is 200 μm).

Figure 2. CD3+ T lymphocyte and Pax-5+ lymphocyte distributions in pig spleen

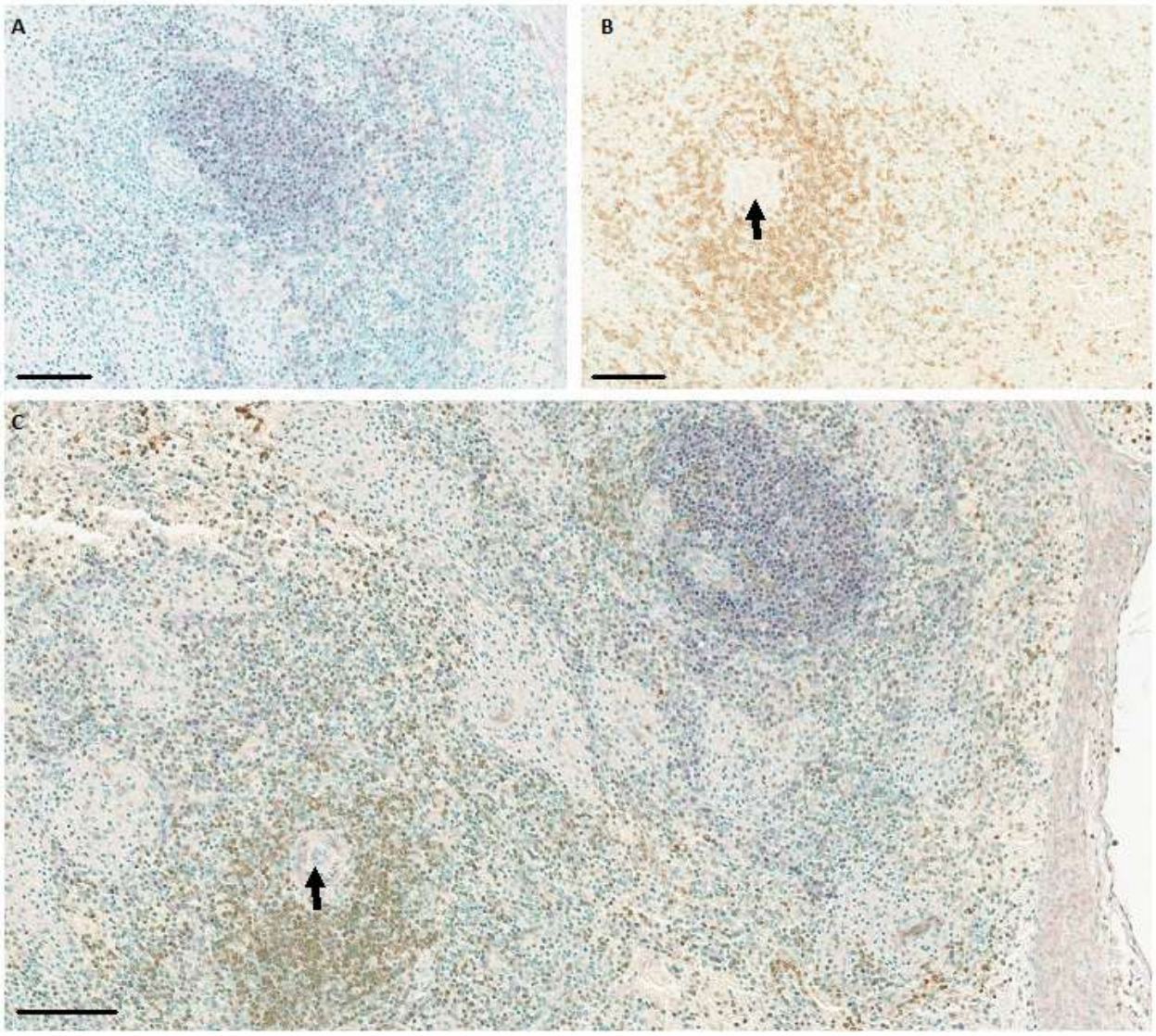

(A) Lymphocytes labeled for Pax-5 nuclear marker (purple) in lymphoid follicles (bar is 100 µm). **(B)** Lymphocytes labeled for CD3 (brown) around PALS (arrow) (bar is100 µm). **(C)** Dual IHC labeling with CD3+ lymphocytes (brown) and Pax-5+ lymphocytes (purple) (bar is 200 µm).

Figure 3. CD3+ and CD4+ T lymphocyte distribution in pig spleen

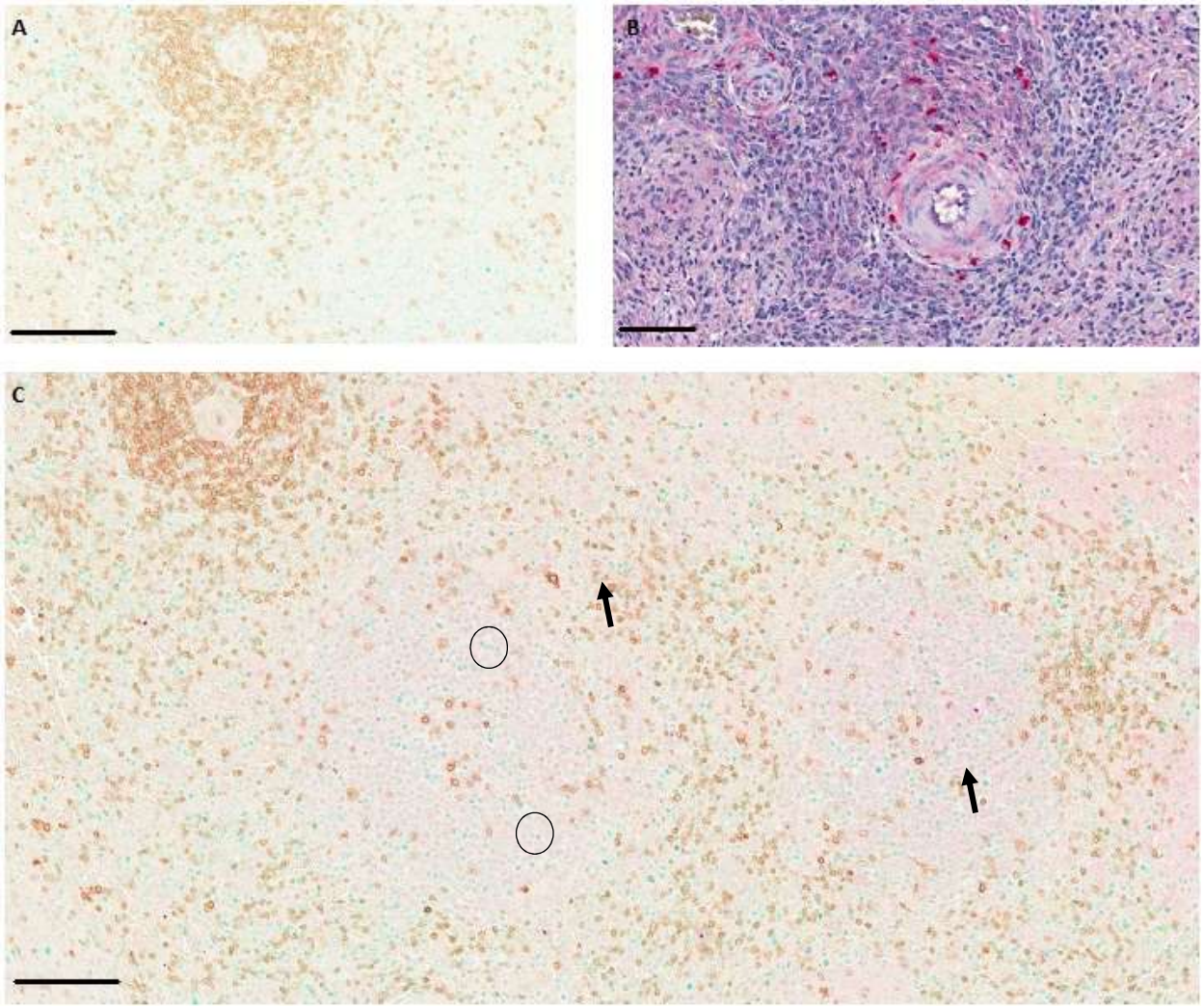

(A) CD3 labeled lymphocytes (brown) (bar is 200 µm), **(B)** CD4 labeled lymphocytes (red) (bar is 100 µm). **(C)** Dual IHC labeling with CD3+ cells (circles) and dual CD3/CD4 labeled cells (arrows) (bar is 200µm).

Chapter 3 - Characterization of Type II Transmembrane Protease, Serine S1 Member 2 (TMPRSS2) Protein and mRNA Expression in Porcine Tissues

Hundreds of proteases can be found in human and animal genomes. The serine protease family is vast and the biological function of many family members has been extensively studied [26]. The discovery of enteropeptidase, the first type II transmembrane serine protease (TTSP), was the beginning of an ever expanding list of TTSPs that are now divided into four groups: human airway trypsin-like/differentially expressed in squamous cell carcinoma (HAT/DESC), hepsin/transmembrane protease serine (hepsin/TMPRSS), matriptase, and corin [27]. Typically synthesized as inactive precursors, each TTSP contains a C-terminal serine protease domain (including histidine, aspartic acid, and serine residues), is rooted in the cellular membrane by an N-terminal transmembrane domain, and has a stem region of varied size [26]. While an initial biological function has been characterized for many of the TTSPs, more recent studies have reported a variety of additional functions throughout the body, including roles in several cancers. Research on the expression of TTSPs has led to the theory that some cancers gain the ability to move through living tissues by leveraging TTSPs' enzymatic activity to damage the extracellular matrix [27].

Structurally, our protease of interest, type II transmembrane protease, serine S1 member 2 (TMPRSS2), includes a serine protease domain, a low-density lipoprotein receptor class A and a cysteine-rich scavenger receptor. [27]. Although little is known about the normal biological function of TMPRSS2, many have characterized its role in cancer [28, 26]. Specifically, TMPRSS2 has been found to be a key catalyst in over expression of androgen associated

transcription factors that aid tumorigenesis in prostate cancer [29]. Beyond the prostate, TMPRSS2 is widely expressed in both human and mouse tissues including the respiratory tract, gastrointestinal tract, urogenital tract, and many endocrine/exocrine tissues [9]. The discovery of TMPRSS2 expression in airway epithelium [8], led to the examination of TMPRSS2's role in respiratory virus activation [30-32].

Viruses require a host cell to replicate and consequently spread, and in some cases as a result cause disease. Viruses use various host cell proteases to activate themselves and cellular expression of these proteases can be the determining factor of pathogenicity [29]. In particular, TMPRSS2 can activate multiple respiratory viruses including: influenza A viruses, coronaviruses and members of *Paramyxoviridae* [33]. Influenza A virus (IAV), a member of *Orthomyxoviridae*, is a segmented, single-stranded, negative-sense, enveloped RNA virus. Its envelope, derived from its host cell's plasma membrane during the process of budding, is studded with the transmembrane spike-shaped glycoproteins, hemagglutinin (HA) and neuraminidase (NA). Together the HA and NA subtypes, numbering 18 and 11 respectively, determine the subtype of influenza virus [34]. Influenza relies on the cleavage of the inactive HA precursor protein, HA0, by host cell proteases into HA1 and HA2 to become infectious [35] and multiple studies have confirmed TMPRSS2's ability to cleave HA0 *in vitro* in human and porcine cell lines [30, 36, 37].

In *vivo* studies with TMPRSS2 gene (*TMPRSS2*) knock-out (KO) mice, reveal that mice lacking this protease have normal development and survival rates [11]. However, they become resistant to many influenza strains including human A/H1N1 and A/H3N2 and avian A/H7N9, a zoonotic influenza virus found in Asia [33, 37-39]. However, although mice are an important experimental animal model for influenza research, they are not naturally susceptible to human

IAV strains, and their responses to influenza infections are not clinically representative of human infections [40].

In contrast, swine are naturally susceptible to human IAV and vice versa, hence they are potentially a better experimental animal choice for researching human IAV. Not unexpectedly, Pietsch et al. 2014 demonstrated that porcine and human TMPRSS2 can both activate IAV in the same way as mouse TMPRSS2 [42]. Unfortunately, to our knowledge, extant information regarding TMPRSS2 expression in swine is currently limited to its confirmed presence in primary cell cultures of porcine tracheal and bronchial epithelial cells [41]. Recently, *TMPRSS2* was knocked out in the pig using CRISPR/Cas9 genome editing [43]. Like KO mice, pigs lacking *TMPRSS2* are phenotypically and reproductively normal. Given the apparent normality of *TMPRSS2* KO mice and swine, the protease is likely functionally redundant *in vivo* and consequently it has potential as an antiviral target [11].

Further study of TMPRSS2's role in respiratory virus infections in pigs requires a detailed understanding of TMPRSS2's expression throughout the respiratory tract. Also, TMPRSS2 expression pattern information in extra-pulmonary organ systems would be of potential value to other infectious disease and cancer research, including the study of porcine epidemic diarrhea virus (PEDV) [44]. Therefore, the objective of this study was to characterize the expression of both TMPRSS2 (protein) and *TMPRSS2* (mRNA) in normal porcine tissues and compare these findings to existing data on their human and mouse tissue expression.

Materials and Methods

Pig tissues

Macroscopically normal tissues were collected from 4 White Crossbred 11-month-old pig (*Sus scrofa*) cadavers of untreated pigs from an unrelated, contemporaneous study at Kansas

State University College of Veterinary Medicine. The tissue samples included: nasal planum and nostril, larynx, trachea, primary bronchus, lung, tongue, esophagus, stomach, small intestine, large intestine, kidney, ureter, urinary bladder, adrenal, liver, pancreas, skin, diaphragm, skeletal muscle, heart, spleen, lymph node, tonsil, and eye. After fixation in 10% neutral buffered formalin, tissues were trimmed into roughly 3mm-thick sections, positioned in histologic cassettes, returned to formalin, and submitted to the KS Veterinary Diagnostic Laboratory's Histopathology Laboratory for routine processing and embedding into paraffin blocks. Hematoxylin and eosin stained slides were reviewed to ensure that the tissues were microscopically normal.

Immunohistochemistry

Tissue blocks were sectioned at 4 μm onto positively charged slides for use in immunohistochemistry (IHC). The protocol development included testing of two different avidin-biotin complex horseradish peroxidase (HRP) detection kits, VECTASTAIN Rabbit ABC HRP kit (PK-4001, Vector Laboratories (VL); Burlingame, CA) and a VECTASTAIN Rabbit ABC Elite kit (PK-6102, VL), as well as a range of the primary antibody dilutions (1:250 to 1:25000 in TBS 1x). For the final IHC runs, samples were deparaffinized in xylenes, rehydrated through graded ethanols (100%, 95%, 70%) at 5 min intervals, heat induced antigen retrieved by vegetable steamer technique in sodium citrate pH 6.0 buffer for 30 min, and cooled for 15 min. Inter-step washes were with 1x tris buffered saline with 0.01% tween-20 (TBSt) unless otherwise specified. The tissues were incubated in 3% hydrogen peroxide (diluted in distilled (DI) water) for 10 min to block endogenous peroxidases. To block nonspecific antibody binding, a 2.5% normal horse serum was applied to tissues for 20 min. Rabbit monoclonal anti-TMPRSS2

(92323, Abcam; Cambridge, MA) antibody diluted 1:2500 in 1x TBS was incubated on tissues for 1 hr at room temperature. VL PK-6102 kit biotinylated secondary antibody then ABC Elite reagent were applied to tissues for 30 min each. The TMPRSS2 antigen was visualized with a 2 min incubation in 3,3'-diaminobenzidine tetrahydrochloride (DAB) (SK-4100, VL) and washed in DI water for 5 min. Slides were counterstained with Mayer's hematoxylin, dehydrated through graded alcohols (70%, 95%, 100%) using 2-min intervals, cleared in xylene, and mounted using Permount mounting medium (SP15-500, Thermo Fisher; Waltham, MA).

In situ hybridization methods

Per our request, Advanced Diagnostics (ACD) manufactured an RNAscope ISH probe (568301, ACD; Hayward, CA) targeting nucleotides 776-1761 of pig *TMPRSS2* gene sequence (XM_021071009.1). Per ACD recommendation, the ISH assay positive and negative control probes used were peptidylprolyl isomerase B (*ppiB*), a pig housekeeping gene, and dihydrodipicolinate reducatase B of *Bacillus subtilis,* respectively.

RNAscope® 2.5 High Definition (HD)—BROWN kit (322310, ACD) was used per the manufacturer's instructions. Specifically, all FFPE tissue blocks from two pigs were sectioned onto positively charged slides with clean technique to avoid RNA contamination and baked at 60ºC for 1 hr. Clean technique includes surface decontamination of the histotome with 70% ethanol, changing the histotome blade between each tissue block and wearing gloves. Tissues were deparaffinized by immersing them in xylenes twice for 5 min, placed in 100% ethanol twice for 1 min each, and air dried for 5 min at room temperature. RNAscope® 2.5 Universal Pretreatment Reagents (322380, ACD) contains all solutions used prior to probe application. To block endogenous peroxidases, tissues were incubated with RNAscope hydrogen peroxide solution for 10 min at room temperature and washed with DI water. Slides were immersed in

100ºC 1X kit target retrieval solution for 15 min and washed with DI water. Slides were then transferred to 100% ethanol for 3 min, dried at 60ºC, and tissues outlined using a hydrophobic pen. Protease Plus solution was applied to the tissues for 15 min at 40ºC in a HybEZ II oven (PN 321710/321720, ACD). After a DI water wash, preheated (40ºC) TMPRSS2 probe and control probes were placed on designated tissue sections and incubated for 2 hr in the HybEZ II oven and washed in 1× Wash Buffer twice for 2 min. The tissues were hybridized using Amp 1 solution for 30 min, Amp 2 solution for 15 min, Amp 3 solution for 30 min and Amp 4 solution for 15 min, all at 40ºC in the HybEZ II oven with 2 washes in 1× Wash Buffer for 2 min after each step. The tissues were incubated with Amp 5 solution for 30 min and Amp 6 solution for 15 min at room temperature with 2 washes in 1× Wash Buffer for 2 min after each step. The bound and amplified probes were visualized with DAB solution, applied for 10 min at room temperature, and slides were rinsed in tap water. Lastly, slides were dehydrated in 70% ethanol for 2 min, 95% ethanol twice for 2 min each, cleared in xylene for 5 min, and mounted using Permount mounting medium.

Results

The TMPRSS2 IHC labeled a variety of cells across multiple tissue types. However, in some organs, a faint diffuse non-specific background was also present in a diversity of cells' nuclear or cytoplasmic compartments, and occasionally both. Adjustments to the primary antibody concentration and antigen retrieval methods did not reduce this background. Consistently, adipose tissue was also nonspecifically labeled, a common finding in IHC. Universally, across all tissue types, the isotype antibody control exposed tissues were devoid of any detectable chromogen staining.

Similarly, *TMPRSS2* ISH labeled in a variety of cell types and this correlated well with the anti-TMPRSS2 IHC signal. As expected, the positive control probe labeling was observed in the nuclei and cytoplasm of cells universally and the negative control probe failed to label any tissues. Nonspecific background was minimal.

Respiratory tract

Both TMPRSS2 and *TMPRSS2* labeling was observed throughout the respiratory tree and the epithelial cells of the submucosal seromucous glands and ducts **(Table 3; Figure 4 and 5)**. There was strong cytoplasmic and only occasional nuclear expression of TMPRSS2 antigen. Consistently, TMPRSS2 labeling was equivalent or stronger in these glandular tissues than in the nearby respiratory epithelial cells. However, *TMPRSS2* signal, while present in the nasal planum and laryngeal submucosal glands, was less prominent relative to nearby respiratory epithelium in the trachea and bronchi. The nasal planum, nostril and laryngeal mucosal epithelia had cytoplasmic and nuclear TMPRSS2 labeling. **(Figure 4A and 4C)**. This expression was strongest in the basal layer and faded out apically. In contrast, *TMPRSS2* expression was strongest apically and became progressively rarer to absent with progression towards the basal lamina **(Figure 4B and 4D)**. In the pseudostratified tracheal and bronchial epithelia, goblet, ciliated columnar and basal epithelial cells all expressed TMPRSS2 **(Figure 4E and 4G).** However, while ciliated and goblet cells both expressed *TMPRSS2,* basal cells rarely expressed this mRNA **(Figure 4F and 4H)**. For both TMPRSS2 and *TMPRSS2*, this pattern continued in the secondary and tertiary bronchi **(Figure 4A and 4B).** Similar expression was seen in the bronchioles and rare non-cell associated protein signal was present in the bronchiolar lumens **(Figure 5A).** Within the pulmonary alveoli, there was widespread differential TMPRSS2 **(Figure 5A and 5C)** and *TMPRSS2* **(Figure 5B and 5D)** labeling of both type I and type II

pneumocytes, with labeling of type II pneumocytes predominating **(Figure 5D, star)**. Labeling of cells morphologically consistent with alveolar macrophages was rare.

Gastrointestinal tract

TMPRSS2 and *TMPRSS2* expression was present throughout the gastrointestinal (GI) tract (**Table 4**). There was rare labeling of gut associated lymphoid tissue (GALT) lymphocytes. In contrast, there was no TMPRSS2 or *TMPRSS2* labeling in the muscularis mucosa, submucosal connective tissue and muscularis propria. TMPRSS2 antigen was present predominantly within the cytoplasm and only occasionally in the nucleus, unless otherwise stated.

The dorsal and ventral epithelial surfaces of the tongue were TMPRSS2 antigen positive. However, in both, the IHC signal was strongest in the stratum basale, weaker in the stratum spinosum, and absent in the stratum granulosum and stratum corneum (**Figure 6A and 6C**). In contrast, *TMPRSS2* expression in the dorsal aspect of the tongue was observed primarily in the stratum spinosum and stratum granulosum, to a lesser degree in the stratum basale, and was completely absent in the stratum corneum (**Figure 6B**). Demarcation of the stratum granulosum and stratum spinosum was harder to appreciate in the ventral lingual aspect, but *TMPRSS2* expression appeared to be similar to that in the dorsal epithelium (**Figure 6D**). TMPRSS2 antigen distribution in the esophagus was observed throughout all the layers of the epithelium except for the stratum corneum, which was devoid of detectable signal. The strongest labeling was in the stratum basale and the signal faded apically. For *TMPRSS2* expression, the signal was weaker and fewer cells labeled positively. TMPRSS2 antigen was strongest in the epithelial cells of the submucosal gland ducts in the esophagus. However, it was also observed in the submucosal glandular epithelium (**Figure 6E**). Similarly, submucosal glands and ducts expressed *TMPRSS2* with the signal stronger in the duct cells (**Figure 6F**).

In all three regions of the stomach, TMPRSS2 and *TMPRSS2* were highly and similarly expressed **(Figure 7)**. In the cardiac and pyloric regions, cytoplasmic protein expression was stronger in the glands of gastric pits with some weak non-cell associated signal also present in the lumens of the gastric glands (**Figure 7A and 7C**). Conversely, *TMPRSS2* was stronger at the apical aspect of the gastric pits and weaker in gastric glands (**Figure 7B and D**). However, both the IHC and ISH labeling were weaker in the pyloric region compared to the cardiac region (tissue examined on the same slide). The pyloric and cardiac regions labeled equivalently to the fundic region for both TMPRSS2 and *TMPRSS2*. In the fundus, many cell types that make up the fundic glands were antigen positive. This labeling was strongest in the chief cells followed by the parietal cells and weakest and only occasionally present in mucosal neck cells (**Figure 7E**). In contrast, *TMPRSS2* was present and of consistent strength across these cell types (**Figure 7F**). The base of the fundic glands had varying levels of TMPRSS2 and *TMPRSS2* expression in the mucous secreting cells, with some cells lacking expression entirely.

Similar expression patterns in the mucosal epithelium of the small intestine (SI) and the large intestine (LI) were observed (**Figure 8**). However, the *TMPRSS2* expression was stronger in LI sections compared to SI sections on the same slide. Throughout the SI, the enterocytes of both the villi and the crypts of Lieberkuhn expressed TMPRSS2. Occasional goblet cells lacked TMPRSS2 expression entirely. There was non-cell associated TMPRSS2 antigen present throughout the intestinal lumen immediately adjacent to the epithelium. In the duodenum, protein expression was stronger in enterocytes' cytoplasm and weaker in the cytoplasm of the submucosal gland cells **(Figure 8A)**. There were clusters of cells with weak protein and mRNA expression in the epithelial lamina propria of the jejunum as well as in ileal villi **(Figure 8C and 8D).** Colonic enterocytes had weak TMPRSS2 expression **(Figure 8E)**. The spiral colonic

epithelium *TMPRSS2* expression was stronger than that of the transverse colon and in both expressions was stronger at the apical aspect **(Figure 8F)**.

Urogenital tract

The kidney, urinary bladder, and ureter as well as uterus all expressed TMPRSS2 protein and mRNA (**Table 5**). Expression of protein and mRNA was absent in glomeruli apart from occasional non-cell associated TMPRSS2 antigen present in Bowman's spaces. There was differential labeling of the convoluted tubules of the cortex, with stronger cytoplasmic TMPRSS2 antigen labeling in the proximal convoluted tubules (PCT) compared to the distal convoluted tubules (DCT) (**Figure 9A**). Conversely, *TMPRSS2* expression was stronger in the DCT compared to PCT (**Figure 9B**). Protein in the lumens of the PCTs labeled strongly for TMPRSS2 antigen. Similar labeling, while present, was weaker and rarer in the lumens of DCTs. In the medulla, the tubular epithelium of the collecting ducts expressed TMPRSS2 and *TMPRSS2*; however, expression was not observed in the loops of Henle and medullary straight proximal tubules (**Figure 9C and 9D**). Both TMPRRS2 and *TMPRSS2* expression was disseminated and strong in the transitional urothelium of the renal pelvis, urinary bladder, and ureter (**Figure 9E, 9G**). No male reproductive samples were available for review. Cells of the uterine mucosal and glandular epithelium expressed TMPRSS2, in the cytoplasm and occasionally nucleus, as well as *TMPRSS2* (**Figure 10A, 10B**). Oocytes in the ovary expressed TMPRSS2 (**Figure 10C**) but due to tissue damage during ISH, *TMPRSS2* expression could not be determined. The stroma was negative in both tissues. Finally, smooth muscle layers throughout the urogenital tract were devoid of signal, a similar pattern to that for smooth muscle throughout the rest of the examined pig tissues.

Additional tissues

Findings for the rest of the examined tissues are detailed in **Table 6**. In skin, there was IHC labeling in all the epithelial layers except the stratum corneum **(Figure 11A)**. TMPRSS2 expression was occasionally nuclear, in addition to cytoplasmic, in the stratum spinosum, stratum granulosum, and stratum lucidum. In contrast, TMPRSS2 was rarely observed in these layers and the stratum basale were negative **(Figure 11B)**. Elsewhere in the skin TMPRSS2 expression was consistently cytoplasmic. Expression of *TMPRSS2* was detected in the outer root sheath of hair follicles **(Figure 11D)**. TMPRSS2 expression mirrored this **(Figure 11C)**. In contrast, the inner root sheath and fibrous sheath were devoid of IHC and ISH signal. The cells lining the apocrine glands of the dermis intense labeling in skin. There was weak, widespread *TMPRSS2* expression in the serous glands and that intensified in the associated ducts **(Figure 11F)**, while TMPRSS2 expression was nuclear and cytoplasmic and of consistent intensity in both glands and ducts **(Figure 11E)**.

The exocrine and endocrine portions of pancreatic tissue expressed TMPRSS2 and *TMPRSS2*. Weak cytoplasmic and rarely nuclear TMPRSS2 and rare *TMPRSS2* expression was occasionally observed in Islet of Langerhans cells **(Figure 12A and 12B)**. TMPRSS2 and *TMPRSS2* labeling in acinar cells that comprise the exocrine tubuloacinar glands was also detected. Protein expression was predominantly cytoplasmic in most acinar cells, with occasional nuclear staining, but approximately 10% of acinar cells were negative. Both the interlobular and intralobular ducts highly expressed TMPRSS2, seen as widespread strong cytoplasmic labeling **(Figure 12C)**. ISH labeling was similar **(Figure 12D)**. Duct lumens occasionally contained TMPRSS2 antigen.

In the liver, bile duct epithelium had very weak cytoplasmic IHC labeling **(Figure 12E)**. In contrast, *TMPRSS2* expression was strong but multifocal **(Figure 12F)**. There was non-cell associated TMPRSS2 antigen present in the sinusoids and lumens of the central and portal veins. Hepatocyte cytoplasm TMPRRS2 labeling was granular. A low level of *TMPRSS2* expression was also present in most hepatocytes, with strong signal in scattered hepatocytes.

In the adrenal, there was weak cytoplasmic, and occasionally nuclear, TMPRSS2 antigen signal in most cells of the zona glomerulosa, zona fasciculata, and zona reticularis of equivalent intensity (**Figure 12G**). However, *TMPRSS2* signal was not observed in any of the cells in the adrenal cortex (**Figure 12H**). In contrast, ganglion cells in the medulla clearly expressed *TMPRSS2*, while IHC labeling was rare and weak **(Figure 12G and 12H).**

Both the red and white pulp of the spleen contained varying levels of IHC and ISH signal. TMPRSS2 expression in leukocytes in the red pulp was typically weak with only occasional strongly positive cells **(Figure 13C)**. Although the ISH signal was difficult to discern in lymphocytes due to the intense hematoxylin staining of the nuclei of cells with scant cytoplasm, it was apparent that some cells weakly expressed *TMPRSS2* **(Figure 13D)**. Protein expression was strongest in and around the lymphoid follicles in the white pulp. Predominantly this was cytoplasmic IHC labeling in the lymphocytes surrounding the periarteriolar lymphoid sheaths (PALS) region, presumably T lymphocytes. Smooth muscle trabeculae, as true for smooth muscle throughout, were negative.

TMPRSS2 and *TMPRSS2* labeling patterns in other lymphoid tissues, including lymph nodes and GALT were consistent with the patterns in the spleen. TMPRSS2 expression was observed most often within the lymphoid follicles as strong cytoplasmic labeling, with

occasional nuclear signal. (**Figure 13A and 13B**). However, labeling in lymph nodes was consistently present yet relatively weak (**Figure 13E and 13F**).

As in other lymphoid tissues, occasional cytoplasmic expression of TMPRSS2 was observed in the tonsillar lymphoid follicles (**Figure 14A**). In contrast, *TMPRSS2* was occasionally in the follicles with rare cells strongly labeled (**Figure 14B**). Tonsillar epithelial cells had positive IHC signal in the stratum basale layer and this signal gradually faded apically with the stratum corneum layer devoid of signal (**Figure 14C**). In contrast, *TMPRSS2* signal was scattered throughout most layers, except the stratum basale and stratum corneum (**Figure 14D**). Interestingly, IHC signal in the stratum basale and most cells in the stratum spinosum was predominantly cytoplasmic. However, the stratum granulosum had very weak TMPRSS2 expression and it was stronger in the nucleus while weaker in the cytoplasm. Diffusely, the tonsillar crypt epithelium was intensely positive, in both the cytoplasmic and nuclear compartments. Although less cells labeled positive for *TMPRSS2*, expression was present in all epithelial layers except the basal layer. Finally, all layers of the corneal epithelium expressed TMPRSS2 (not pictured). However, due to technical difficulties, ISH analysis was not possible.

Discussion

We found that TMPRSS2 and its corresponding mRNA (*TMPRSS2*) were highly expressed throughout swine tissues, especially in the respiratory, urogenital, and gastrointestinal tracts. These findings correlate well with existing human and mouse expression pattern data for this protease. Although, our study was prompted by a need to better understand TMPRSS2 expression within the context of influenza pathogenesis for which swine are an important biomedical research animal, we examined expression in a wide variety of additional tissues. To

our knowledge this was the first study, in any species, to provide such a detailed expression profile for this protease.

Specific cell type localization of TMPRSS2 information for both human and mouse tissues is limited because most prior studies rely on mRNA expression analysis alone [45]. This limited opportunities to compare the porcine protein expression pattern to that of humans and mice. While there are similarities between mice and humans [23], expression patterns in pigs better correlated to human expression patterns especially in the respiratory, gastrointestinal, and urogenital tracts.

We found many similarities between porcine *TMPRSS2* (*pTMPRSS2*) tissue expression patterns and those of humans and mice [46]. One of the most notable differences for *pTMPRSS2* and human expression in comparison to mouse *TMPRSS2* (*mTMPRSS2*) expression was in the respiratory tract. Previous studies of human respiratory tissues have found *TMPRSS2* expression in submucosal glands and epithelial cells of the nose, trachea, distal airway, alveolar macrophages and type II pneumocytes [8]. In contrast, *mTMPRSS2* is present exclusively in bronchial and bronchiolar epithelium and absent in the alveoli [46]. In the present study, we observed a similar expression pattern for *pTMPRSS2* in the bronchi and bronchioles to that in mice and humans (**Figure 4H**). However, unlike mice and like humans, pig pneumocytes expressed *pTMPRSS2* (**Figure 5D**). This expression was predominantly in cells that were morphologically consistent with type II pneumocytes. However, rare positive cells could have been alveolar macrophages. Co-labeling with anti-TMPRSS2 and a macrophage marker would confirm whether or not macrophages were expressing TMPRSS2.

There are known limitations on the mouse as a model for human influenza and our respiratory tract TMPRSS2 expression findings expand these limitations. Ibricevic et al., 2006

confirmed replication of seasonal H3N2 IAV in ciliated and non-ciliated human respiratory epithelial cell cultures including type II pneumocytes [47]. They determined limitations on the mouse model's fit for purpose for IAV infection studies due to differences in human respiratory epithelium IAV receptor expression. Specifically, mice lack the α2,6-linked sialic acid (Sia) receptors, expressed by human ciliated and goblet cells throughout the conducting airways, that are critical to establishment of human IAV infections in the upper respiratory tract. In contrast, mice and humans similarly express α2,3-linked Sia receptors in their respiratory epithelium, particularly deep in the respiratory tree on the apical surface of type II pneumocytes within their alveoli. TMPRSS2 activates the influenza A virus (IAV) by cleaving HA0, the inactive HA precursor, into its active forms HA1 and HA2 [34]. In humans, TMPRSS2 is expressed throughout the respiratory tree epithelium including in type II pneumocytes [9]. Working with the TMPRSS2 knock-out mouse model, Tarnow et al., 2014 showed that TMPRSS2 activates seasonal H3N2 IAV in the mouse [38]. However, mice do not express TMPRSS2 in either type I or type II pneumocytes hence this activity was likely restricted to the conducting airways [9]. In contrast, we found that pTMPRSS2 expression in all cell types previously shown to be targeted by human H3N2 IAV in the respiratory tree. This includes the epithelial cells of the trachea (**Figure 4E and 4F**), bronchi (**Figure 4G and 4H**), and pneumocytes of the pulmonary alveoli (**Figure 5C and 5D**). Consequently, not only does the mouse lack the preferred α2,6 Sia receptors for human IAV throughout their respiratory tree, but their type II pneumocytes lack TMPRSS2 expression. In contrast, the expression of both α2,3 and α2,6 Sia throughout the porcine respiratory tract mirrors that in humans as does their TMPRSS2 expression [48].

TMPRSS2 activates other respiratory viruses including parainfluenza viruses [49], coronaviruses [10] and human metapneumovirus [50]. It activates parainfluenza viruses by

cleaving the viral F protein leading to cell-to-cell fusion [51]. Recently, Palinski et al., 2016 determined the widespread presence of porcine parainfluenza virus 1 in US swine herds. Consequently, further research into TMPRSS2's role in parainfluenza infections in pigs has both biomedical and agricultural relevance. In coronavirus infections, TMPRSS2 cleaves the viral spike protein leading to cell-to-virus fusion [51]. This activation mechanism has been confirmed for severe acute respiratory syndrome-related coronavirus (SARS-CoV) [52], Middle East respiratory syndrome-related coronavirus (MERS-CoV) [10] and human 229E [53]. In 2005, Chen et al. determined that pigs were susceptible to human SARS-CoV infections, making pigs a potential model for SARS research [54]. Further characterization of TMPRSS2 in pigs in relation to respiratory infection could greatly aid in the research and development of potential antiviral treatments.

Human TMPRSS2 (*hTMPRSS2*) expression information for both protein and mRNA in the GI tract is limited. According to Bertram et al., 2012, the epithelium of the stomach, ileum, and colon as well as their submucosal glands expressed both *TMPRSS2* and TMPRSS2 in humans [6]. Similarly, we saw strong anti-TMPRSS2 and widespread *TMPRSS2* labeling in epithelial cells and submucosal glands in the esophagus, stomach, ileum, and colon samples. Conversely, *mTMPRSS2* expression has only been reported in the small intestine and stomach [11]. Further information regarding human expression in the GI tract would be needed to complete this comparison.

However, TMPRSS2 expression in the GI tract of pigs also has relevance to porcine infectious disease research. Porcine epidemic diarrhea virus (PEDV), like other coronaviruses, relies on proteolytic cleavage of its spike protein to become infectious [44]. With a mortality rate of up to 100% in piglets, this disease causes significant financial losses. As for influenza, other

host cell proteases can also activate PEDV. However, TMPRSS2 is the only identified host cell protease that appears to lack a necessary physiological role. We found TMPRSS2 expression in small intestinal epithelial cells, PEDV's target cell type. Therefore, further characterization of TMPRSS2's role in PEDV infection is warranted.

We observed expression of TMPRSS2 in cells throughout the liver of the pig. Recently, Esumi et al, 2015 showed that TMPRSS2 successfully activates the flavivirus hepatitis C virus (HCV) *in vitro* and is the only serine protease to be upregulated during chronic HCV infections [55]. Further research might examine which cell types produce *TMPRSS2* and if these cells are secreting TMPRSS2 during HCV infections. Given the public health importance of yellow fever, Japanese Encephalitis, Zika, and Dengue fever, investigation of a potential role for TMPRSS2 in these diseases also caused by flaviviruses would also be apropos.

TMPRSS2 has been reported in mouse and human kidney samples. However, to our knowledge no protein expression information is available [46, 56]. Moreover, *hTMPRSS2* was found in renal tubules, but no data is available on differential expression between proximal and distal convoluted tubules. *mTMPRSS2* expression is reported to be restricted to the distal convoluted tubules (DCT) and collecting ducts [9]. In pigs, we also observed variation in protein and mRNA expression in the renal tubules. However, the pattern was different to that in humans. Porcine proximal convoluted tubules (PCT) expressed higher levels of TMPRSS2 than DCT (**Figure 9A**). Conversely, there were higher levels of *TMPRSS2* expression in the DCT than the PCT (**Figure 9B**).

Many TTSPs are secreted extracellularly [27], for example prostate cancer cells secrete TMPRSS2 [28]. In addition to finding evidence for this in the lumens of PCT, we noted extracellular antigen signal within bronchiolar lumens, Bowman's capsule, liver sinusoids,

gastrointestinal submucosal gland ducts, and many ducts in other tissues. The cells adjacent to this extracellular TMPRSS2 consistently expressed *TMPRSS2* supporting the secretion concept.

This study had limitations. First, cell type identification was restricted to those identifiable by their morphology on a hematoxylin and eosin stain. Further examination of expression patterns using co-labeling with specific cell type markers would provide further detail. Possibilities include co-labeling for type II pneumocytes and macrophages in the lung as well as lymphocyte subset markers in the lymphoid tissues. Second, all study pigs were the same age, 11 months old. Age has been shown to effect protease expression levels in mice [9]. Consequently, characterization of expression pattern differences due to age would be of value. A third limitation is related to the availability of nasal turbinate tissues. The study animals were old enough that their nasal turbinate tissues were not harvested because they would have required extensive decalcification and separate testing of the TMPRSS2 IHC and ISH protocols on decalcified tissues, something outside the scope of the immediate project. A future study on porcine nasal turbinate expression of TMPRSS2 would be of value given the use of the intranasal inoculation route in porcine influenza studies and the role of the nasal turbinate epithelium as a site of active influenza infection for both natural infection and live attenuated vaccines. A fourth limitation stemmed from technical difficulties with delicate tissue types. The corneal epithelium had TMPRSS2 expression, however, due to the harsher antigen retrieval methods required for ISH, post antigen retrieval there was no epithelium to examine. This same loss occurred with ovary. Consequently, there were no ISH results for these tissues. Lastly, our results are descriptive only. Use of quantitative polymerase chain reaction (qPCR), quantitative ISH or IHC digital image analysis would address this issue.

In summary, pTMPRSS2 is expressed in a diversity of cell types and in almost all tissue types examined in this study. While some patterns are consistent across pigs, mice and humans, porcine expression patterns more closely correlated to the human expression patterns rather than mouse. These findings are useful for both infectious disease and cancer research. TMPRSS2 plays a significant role in the activation of influenza. While the mouse is an adequate experimental animal choice for some influenza research [57], differences in its influenza receptor and TMPRSS2 expression [9, 47] limit its usefulness for study of the role of TMPRSS2 in influenza infection. Given the pig's similarities to humans in their influenza receptor and TMPRSS2 expression as well as clinical course of influenza infection, we propose further study of TMPRSS2's role in influenza infection in pigs, including transgenic pigs that lack the TMPRSS2 gene. The close correlations between pig and human TMPRSS2 expression may also warrant use of swine to research other diseases, particularly other respiratory and gastrointestinal viral diseases, as well as to study the still to be elucidated physiological function of TMPRSS2.

Acknowledgements

We thank Izabela Ragan for assistance with tissue collection and Monica Gamez for initial development work on TMPRSS2 IHC and mRNA expression.

Figure 4. TMPRSS2 and *TMPRSS2* expression in upper respiratory tissues

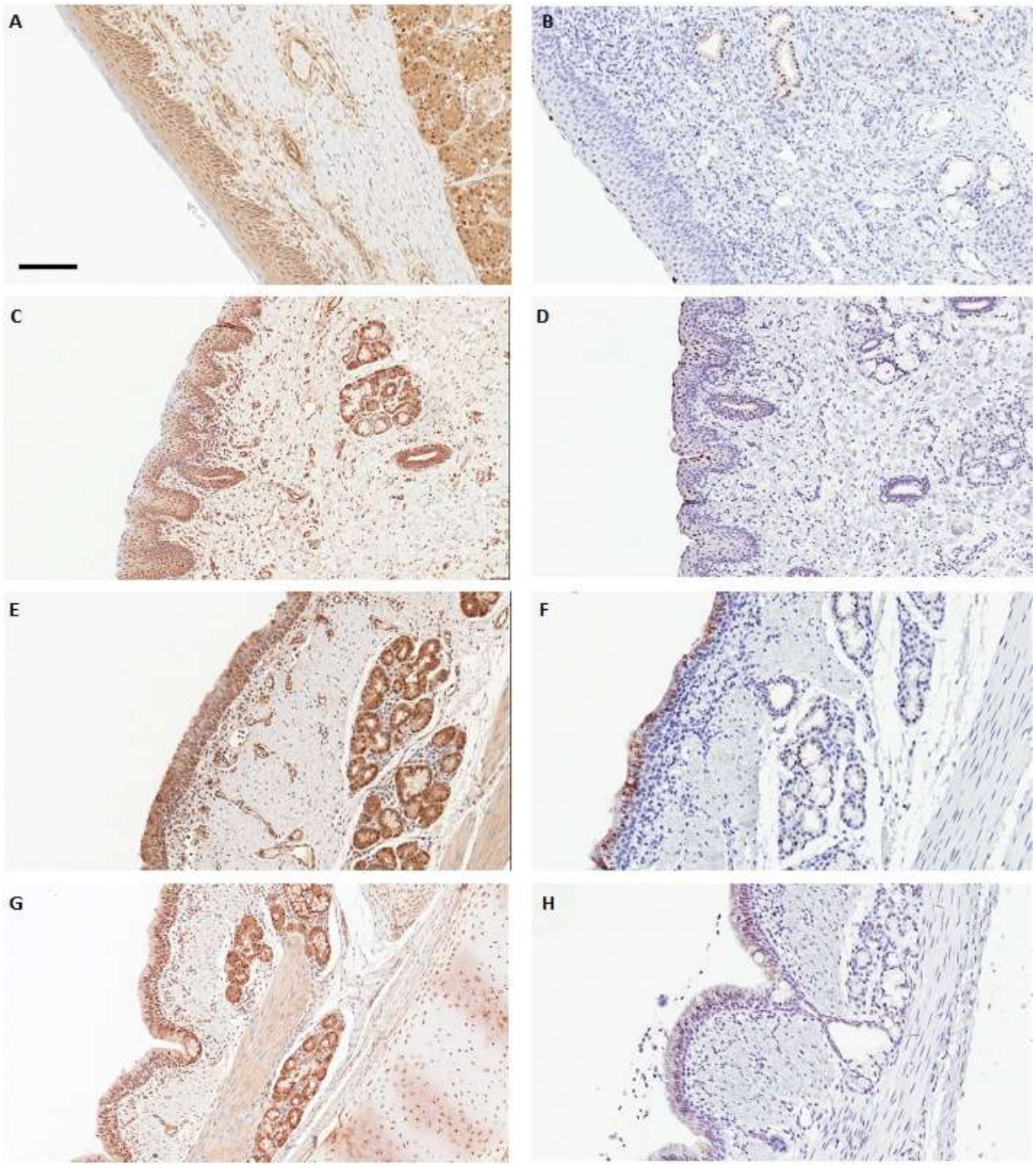

(A) TMPRSS2 expression in nasal planum and nostril epithelia, submucosal glands, and ducts. **(B)** *TMPRSS2* expression in nasal planum and nostril epithelia. **(C)** Expression of TMPRSS2 in laryngeal epithelium, glands, and ducts. **(D)** *TMPRSS2* expression in glands, ducts, and epithelium of the larynx. **(E)** TMPRSS2 expression in tracheal epithelium, glands, and ducts. **(F)** Expression of *TMPRSS2* in tracheal epithelium, glands and ducts. **(G)** Expression of TMPRSS2 in the primary bronchus. **(H)** *TMPRSS2* expression in the primary bronchus. Bar is 100 μm and applies to all images.

Figure 5. TMPRSS2 and *TMPRSS2* expression in lung

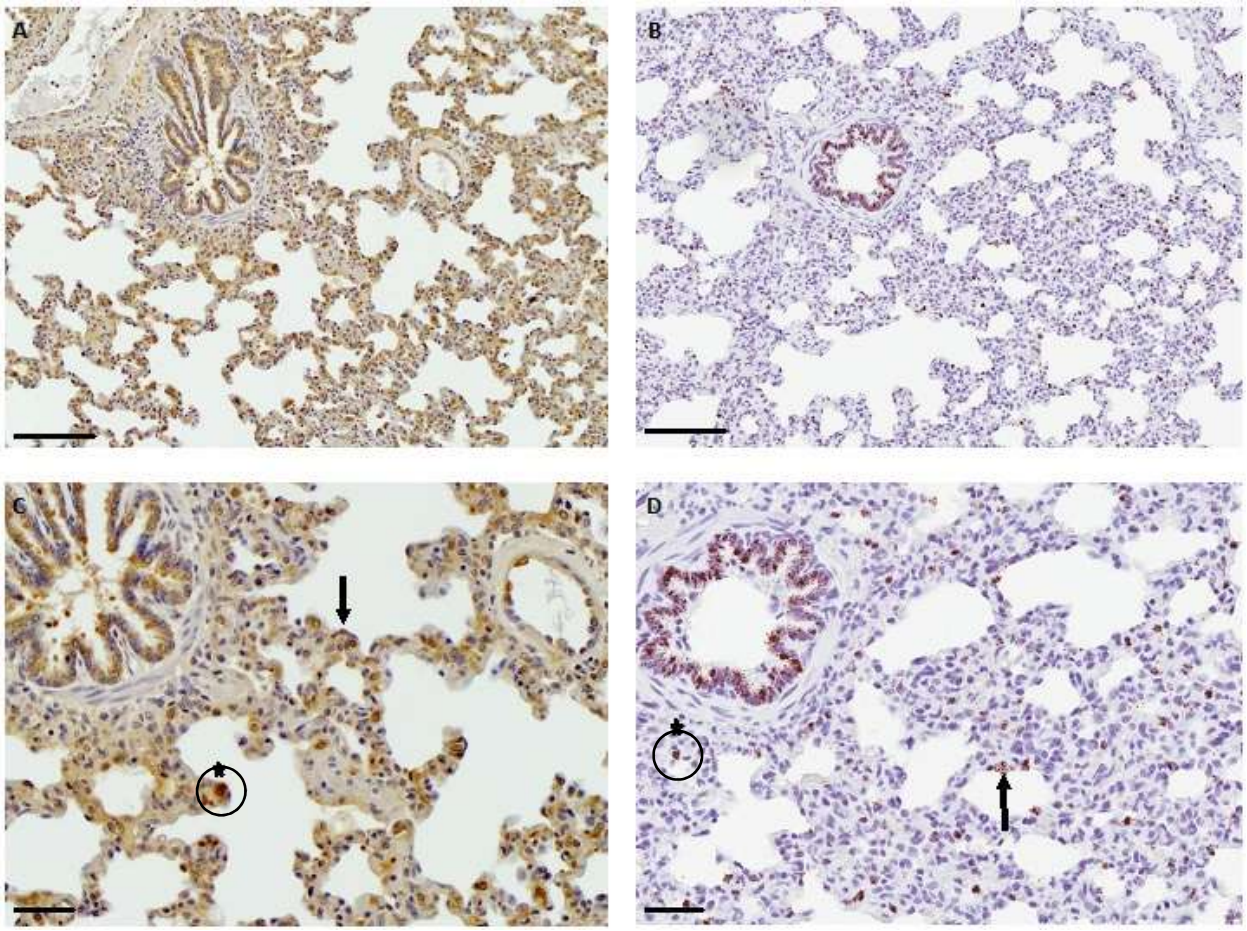

(**A)** Widespread TMPRSS2 antigen labeling in bronchi, bronchioles, alveolar ducts and alveoli with some non-cell associated antigen signal in bronchiolar lumens (bar is 100 μm) (**B)** *TMPRSS2* expression in bronchus, alveolar ducts and alveoli (bar is 100 μm). (**C)** TMPRSS2 expression in the bronchioles and cells morphologically consistent with type I pneumocytes (arrow) and type II pneumocytes (circle) (bar is 50 μm). **(D)** Expression of *TMPRSS2* in the bronchioles and cells morphologically consistent with type I pneumocytes (arrow) and type II pneumocytes (circle) (bar is 50 μm).

Table 3. TMPRSS2 and *TMPRSS2* expression patterns in respiratory tissues

Respiratory tissues	Structure	IHC	ISH
Nasal turbinate	Epithelium	+	R+
	Seromucous glands	+	+
Larynx	Epithelium	+	+
	Seromucous glands	+	+
Trachea	Epithelium	+	+
	Seromucous glands	+	+
Bronchi	Epithelium	+	+
	Bronchial glands	+	+
Pulmonary acinus	Pneumocyte type I	O+	R+
	Pneumocyte type II	+	+
	Macrophage	R+	-
Diaphragm	Myocyte	-	-

(+) = positive, (O+) = occasionally positive, (R+) = rarely positive, (-) = negative

Figure 6. TMPRSS2 and *TMPRSS2* expression in the proximal gastrointestinal tract

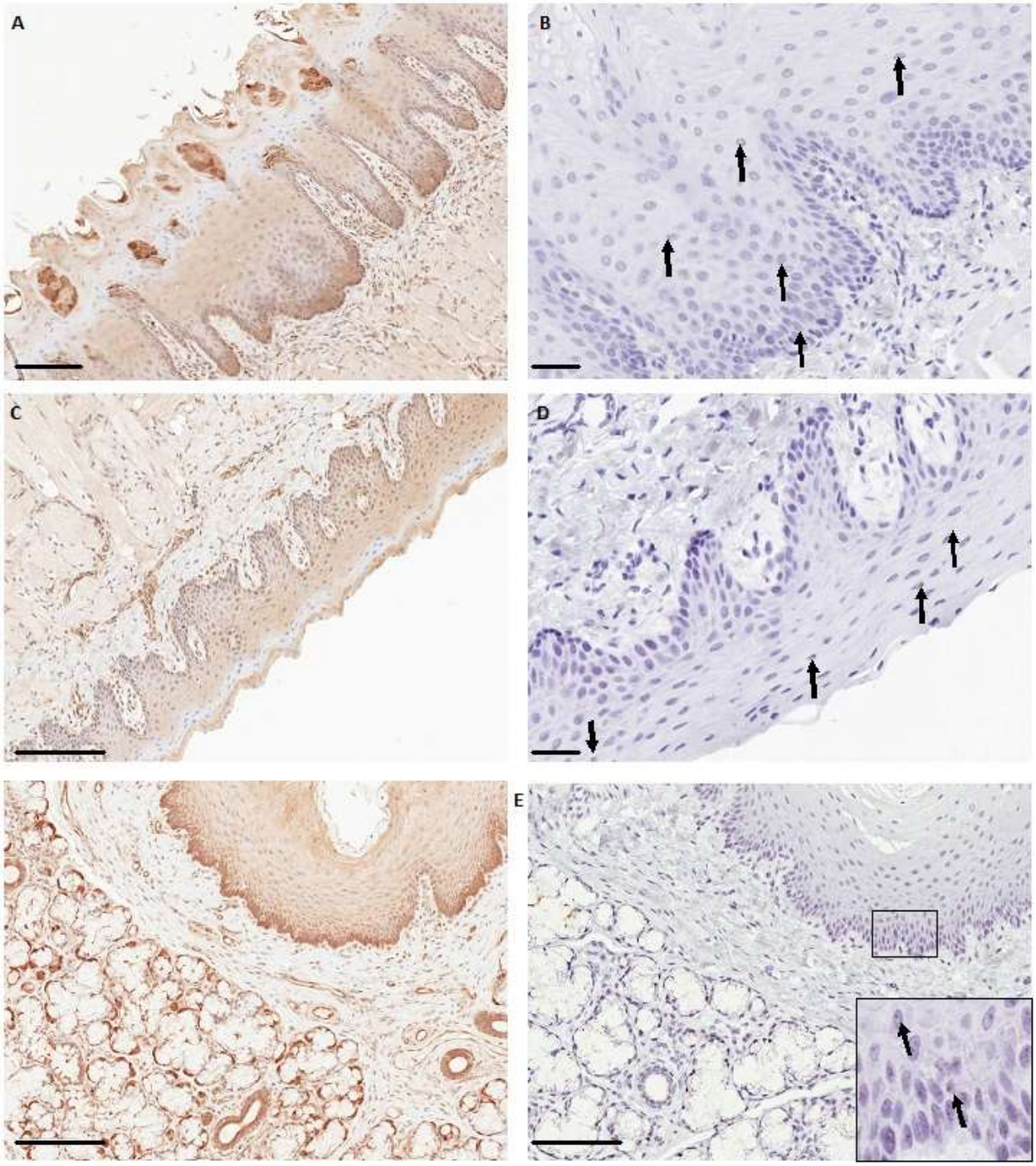

(A) TMPRSS2 labeling in the dorsal tongue epithelium (bar is 100 µm). **(B)** *TMPRSS2* expression in the dorsal tongue epithelium (bar is 50µm). **(C)** TMPRSS2 expression in the ventral aspect of the tongue (bar is 200 µm). **(D)** *TMPRSS2* expression in the ventral tongue epithelium (bar is 50 µm). **(E)** TMPRSS2 expression in the esophageal epithelium, submucosal glands, and ducts (bar is 200 µm). **(F)** *TMPRSS2* expression in the esophageal epithelium, submucosal glands, and ducts (bar is 200 µm).

Figure 7. TMPRSS2 and *TMPRSS2* expression in the stomach

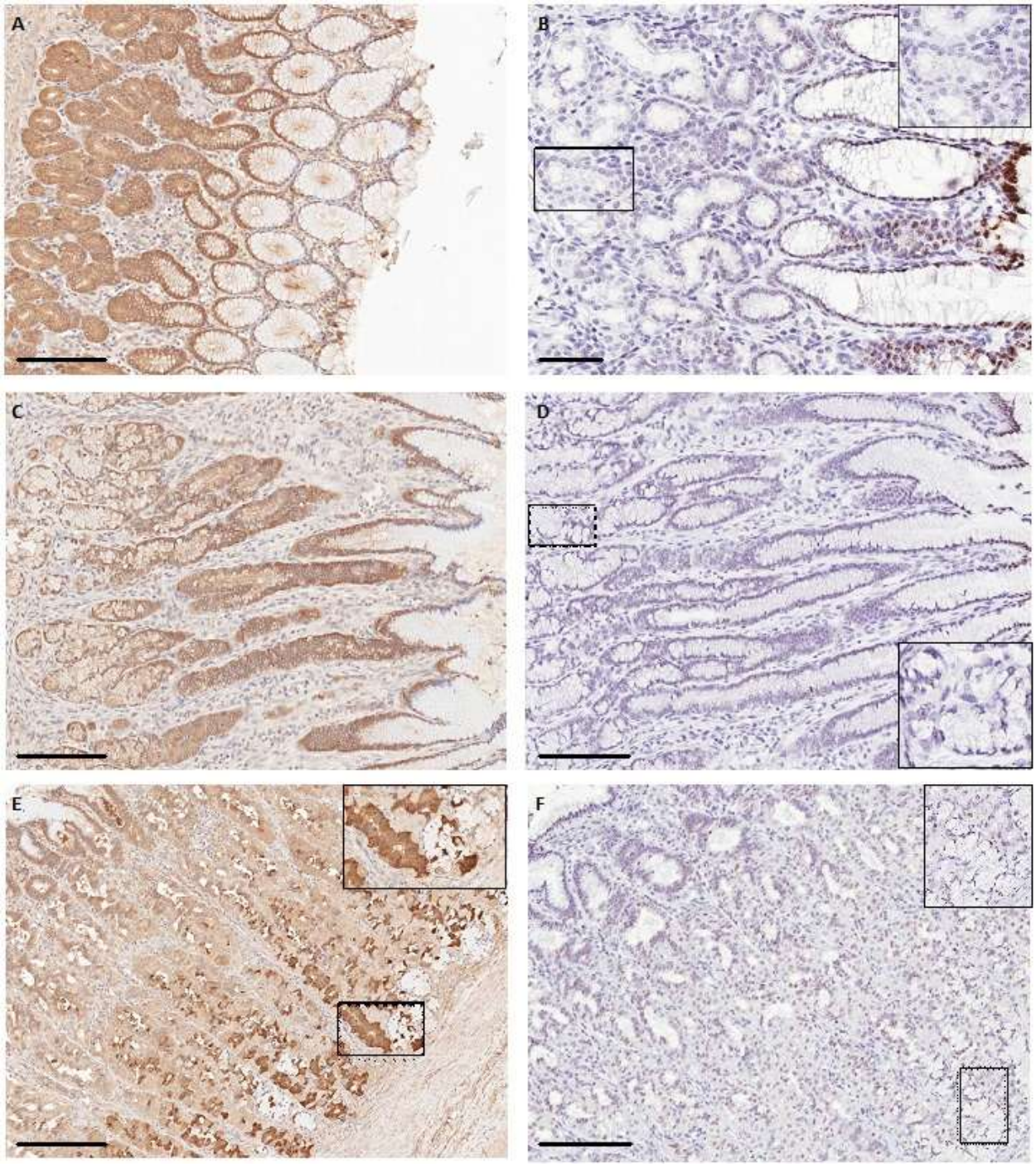

(A) TMPRSS2 expression in the gastric glands and pits of the cardiac region (bar is 200 μm). **(B)** Expression of *TMPRSS2* of the cardiac region in the gastric pits and gastric glands (inset) (bar is 100 μm). **(C)** Expression of TMPRSS2 in the pyloric region was consistent with expression observed in cardiac region (bar is 200 μm). **(D)** Expression of *TMPRSS2* in the pyloric region gastric pits and glands (inset) (bar is 200 μm). **(E)** Expression of TMPRSS2 in the chief (inset), parietal, and mucous neck cells of the fundus region (bar is 200 μm). **(F)** *TMPRSS2* labeling was of consistent strength across all these cell types in the fundus region (bar is 200 μm).

Figure 8. TMPRSS2 and *TMPRSS2* expression in small and large intestines

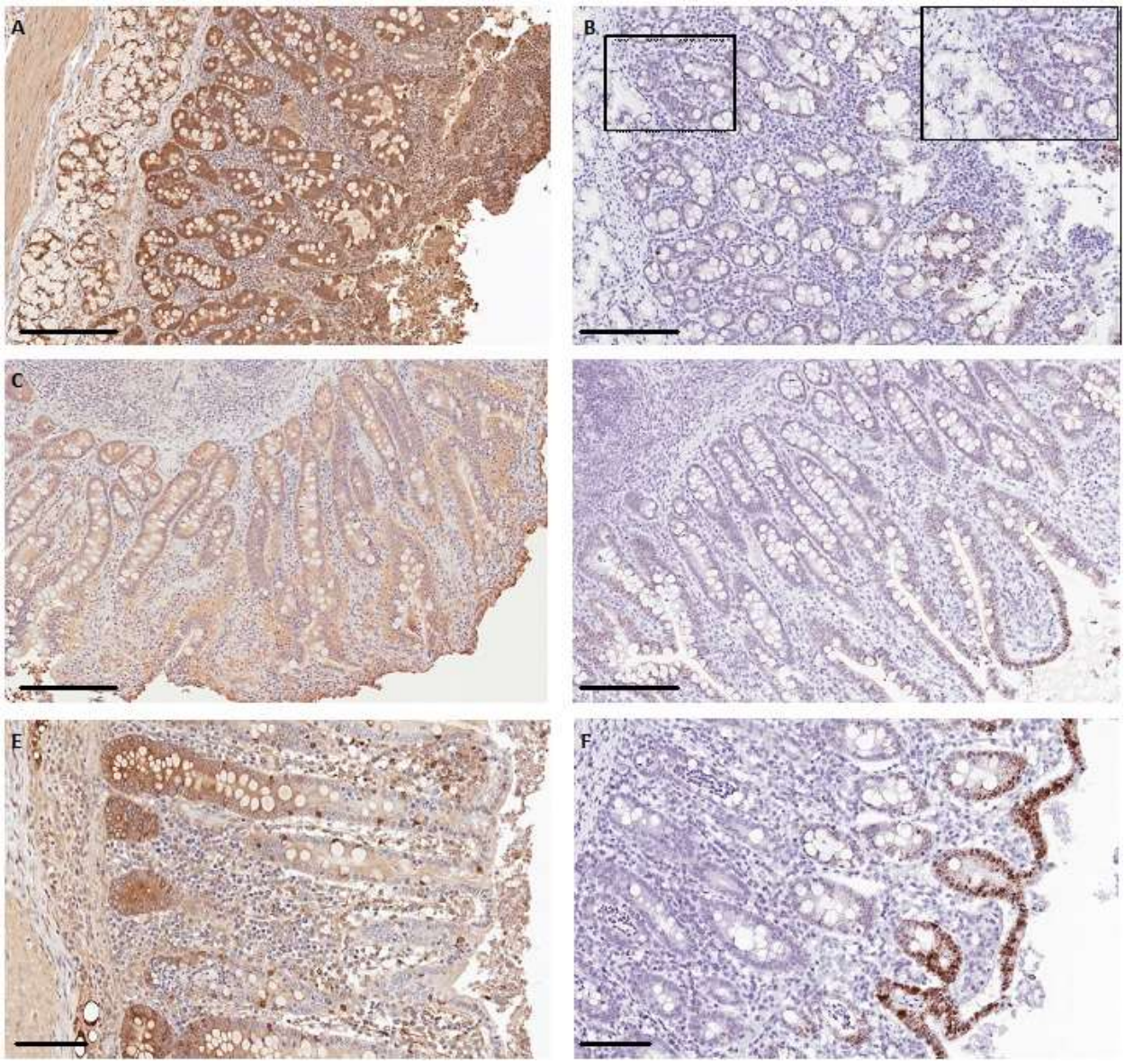

(A) TMPRSS2 labeling of the enterocytes and submucosal glands of the duodenum (bar is 200 µm). **(B)** Expression of *TMPRSS2* in the duodenum with pinpoint expression of consistent strength found in the submucosal glands and enterocytes (inset) (bar is 200 µm). **(C)** TMPRSS2 antigen signal in the enterocytes and the crypts of Lieberkuhn in the ileum (bar is 200 µm). **(D)** *TMPRSS2* expression in ileal enterocytes of the villi compared to the crypts of Lieberkuhn (bar is 200 µm). **(E)** TMPRSS2 expression in the colonic enterocytes (bar is 100 µm). **(F)** *TMPRSS2* labeling of the enterocytes in the colon (bar is 100 µm).

Table 4. TMPRSS2 and *TMPRSS2* expression patterns in gastrointestinal tissues

Gastrointestinal Tissue	Structures	IHC	ISH
Tongue	Dorsal epithelium	+	+
	Ventral epithelium	+	O+
	Skeletal muscle	-	-
Esophagus	Epithelium	+	R+
	Submucosal glands	+	+
	Submucosal ducts	+	+
Fundic stomach	Parietal cells	+	+
	Chief cells	+	+
	Mucosal cells	+	+
	Fundic glands	+	+
Cardiac stomach	Mucosal cells	+	+
	Cardiac glands	+	+
Pyloric stomach	Mucosal cells	+	+
	Pyloric glands	+	+
Duodenum	Enterocytes	+	+
	Goblet cells	-	+
	Submucosal glands	+	+
	Submucosal ducts	+	+
	Lamina propria	+	-
Jejunum	Enterocytes	+	+
	Goblet cells	-	+
	Lamina propria	+	-
	Vascular endothelium	+	-
Ileum	Enterocytes	+	+
	Goblet cells	-	+
	Peyers patches	O+	R+
	Lamina propria	R+	R+
	Vascular endothelium	+	-
Spiral colon	Enterocytes	+	+
	Goblet cells	+	+
Distal colon	Enterocytes	+	+
	Goblet cells	+	+

(+) = positive, (O+) = occasionally positive, (R+) = rarely positive, (-) = negative

Figure 9. TMPRSS2 and *TMPRSS2* expression in renal tissues

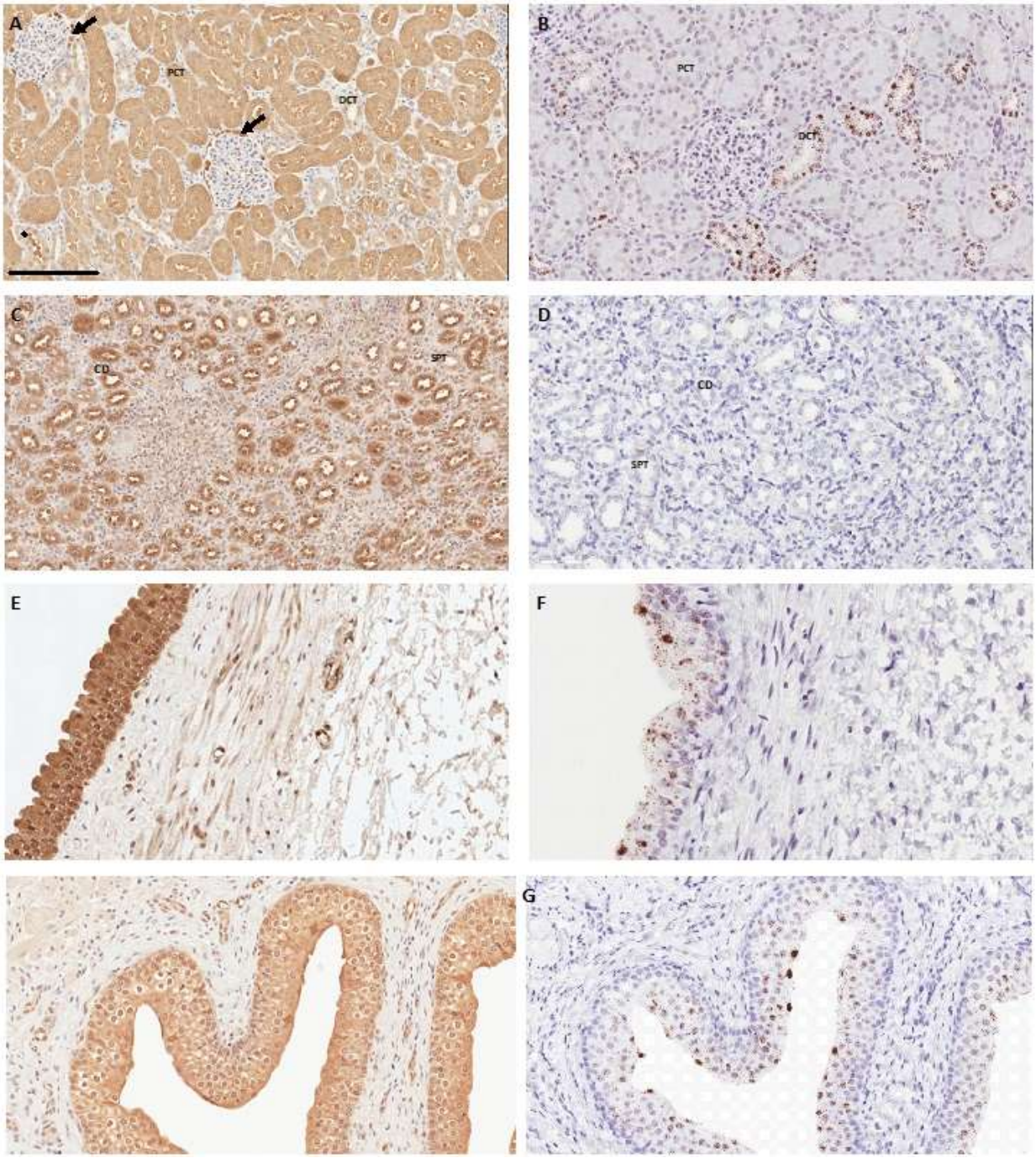

(A) TMPRSS2 antigen labeling of the proximal convoluted tubules (PCT) compared to the distal convoluted tubules (DCT) and extracellular signal in bomans space (arrows), PCT lumens, and DCT lumens (star). **(B)** *TMPRSS2* expression in the DCT compared to PCT. **(C)** TMPRSS2 expression in medullary collecting ducts (CD) and straight proximal tubules (SPT). **(D)** *TMPRSS2* expression in the medullary CD and SPT **(E)** TMPRRS2 expression in the renal pelvic epithelium. **(F)** *TMPRSS2* expression in the epithelium of the renal pelvis. (**G)** Expression of TMPRSS2 in the transitional urothelium of the ureter. **(H)** *TMPRSS2* labeling in the urothelium of the ureter. Bar is 200 μm and applies to all images.

Figure 10. TMPRSS2 and *TMPRSS2* expression in reproductive tissues

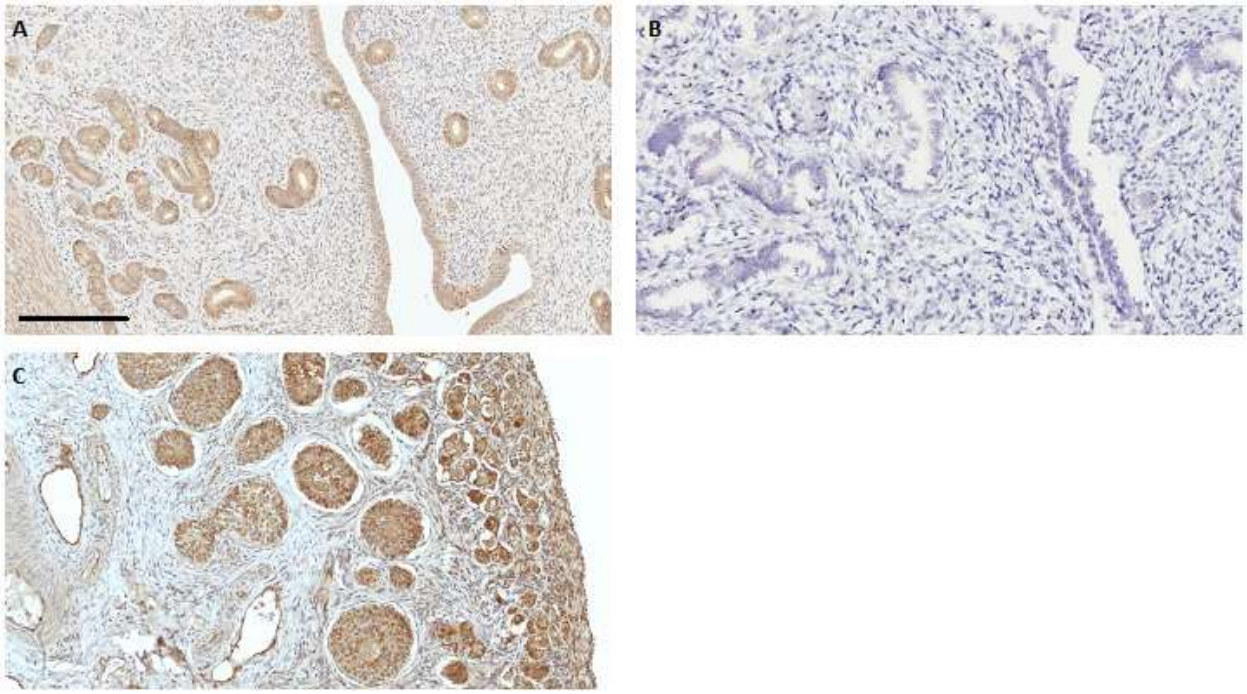

(A) TMPRSS2 in the uterine mucosal and glandular epithelium. **(B)** *TMPRSS2* in the uterine mucosal and glandular epithelium. **(C)** Expression of TMPRSS2 in oocytes of the ovary. Bar is 200 µm and applies to all images

Table 5. TMPRSS2 and *TMPRSS2* expression patterns in urogenital tissues

Tissues	Structure	IHC	ISH
Kidney	Glomeruli	-	-
	Proximal convoluted tubules	+	+
	Distal convoluted tubules	+	+
	Collecting tubules	+	+
	Epithelium	+	+
Ureter	Epithelium	+	O+
Bladder	Epithelium	+	+
Uterus	Epithelium	+	O+
	Endometrial glands	+	+
Ovary	Stroma	-	N/A
	Oocytes	+	N/A

(+) = positive, (O+) = occasionally positive, (-) = negative,
N/A = not available

Figure 11. TMPRSS2 and *TMPRSS2* expression in skin

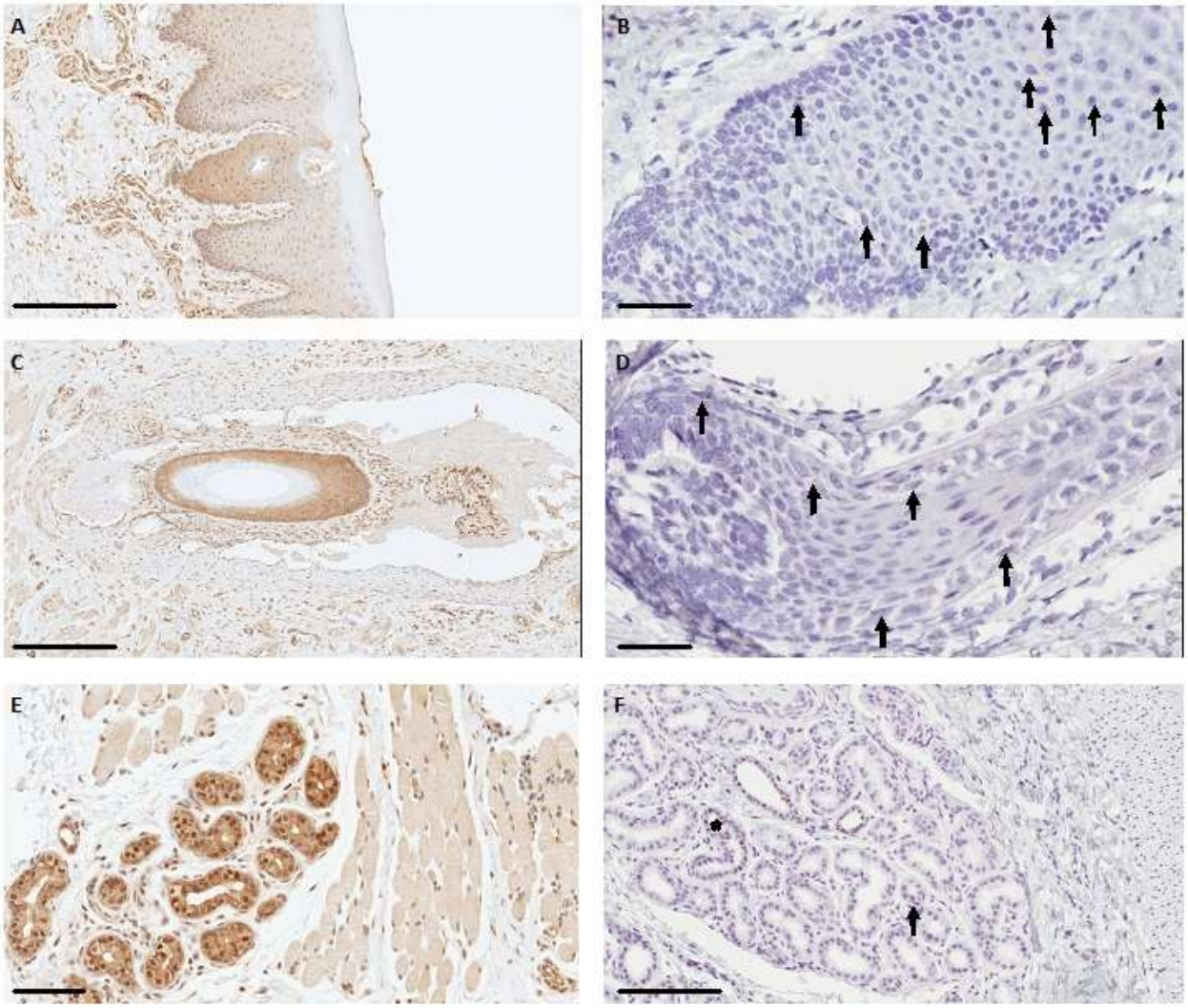

(A) TMPRSS2 antigen signal in the epithelial layers of the skin (bar is 200 μm). **(B)** Occasional *TMPRSS2* expression in layers of skin epithelium (arrows) (bar is 100 μm). **(C)** TMPRSS2 expression in the hair follicle (bar is 200 μm). **(D)** Expression of *TMPRSS2* in the outer root sheath of hair follicles (bar is 100 μm). **(E)** TMPRSS2 expression in the apocrine glands of the dermis (bar is 100 μm). **(F)** *TMPRSS2* expression in the apocrine glands of the dermis (arrow) and associated ducts (star) (bar is 200 μm).

Figure 12. TMPRSS2 and *TMPRSS2* expression in pancreas, liver, and adrenal

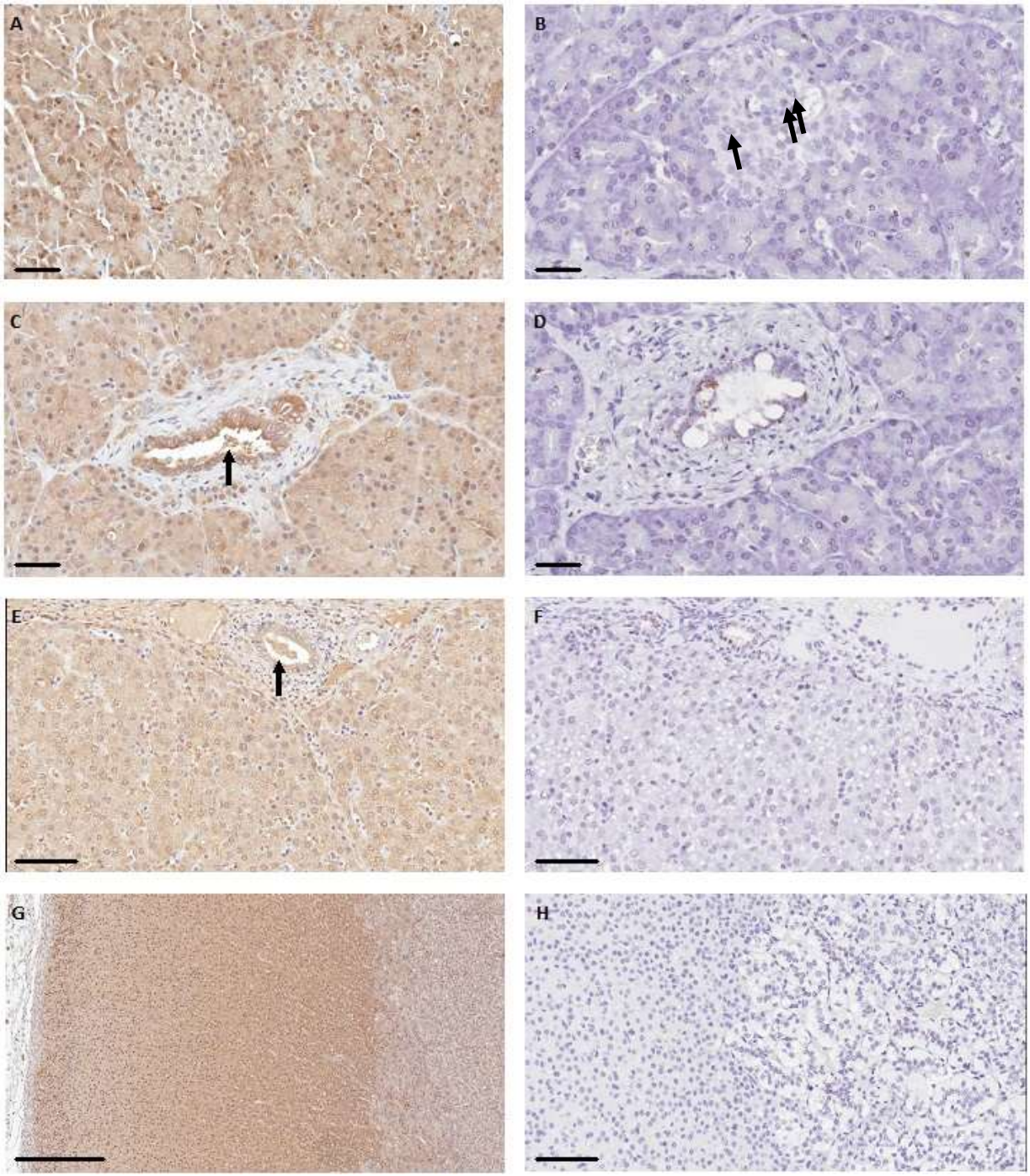

(A) Expression of TMPRSS2 in acinar cells and Islet of Langerhans cells of the pancreas (bar is 100 µm). **(B)** *TMPRSS2* labeling of acinar cells and Islet of Langerhans cells (arrows) (bar is 100 µm). **(C)** TMPRSS2 antigen labeling in both the pancreatic interlobular and intralobular ducts with occasional non-cell associated protein signal in pancreatic duct lumens (arrow) (bar is 100 µm). **(D)** *TMPRSS2* expression in pancreatic ducts (bar is 100 µm). **(E)** Expression of TMPRSS2 in hepatocytes, bile duct epithelium, and non-cell associated signal in the lumen (arrow) (bar is 200 µm). **(F)** *TMPRSS2* signal in hepatocytes and epithelial duct cells (bar is 200 µm). **(G)** TMPRSS2 antigen signal in cells adrenal cortical cells as well as medullary ganglion cells (bar is 300 µm). **(H)** *TMPRSS2* expression in the adrenal cortical cells as well as medullary ganglion cells (bar is 200 µm).

Figure 13. TMPRSS2 and *TMPRSS2* expression in lymphoid tissues.

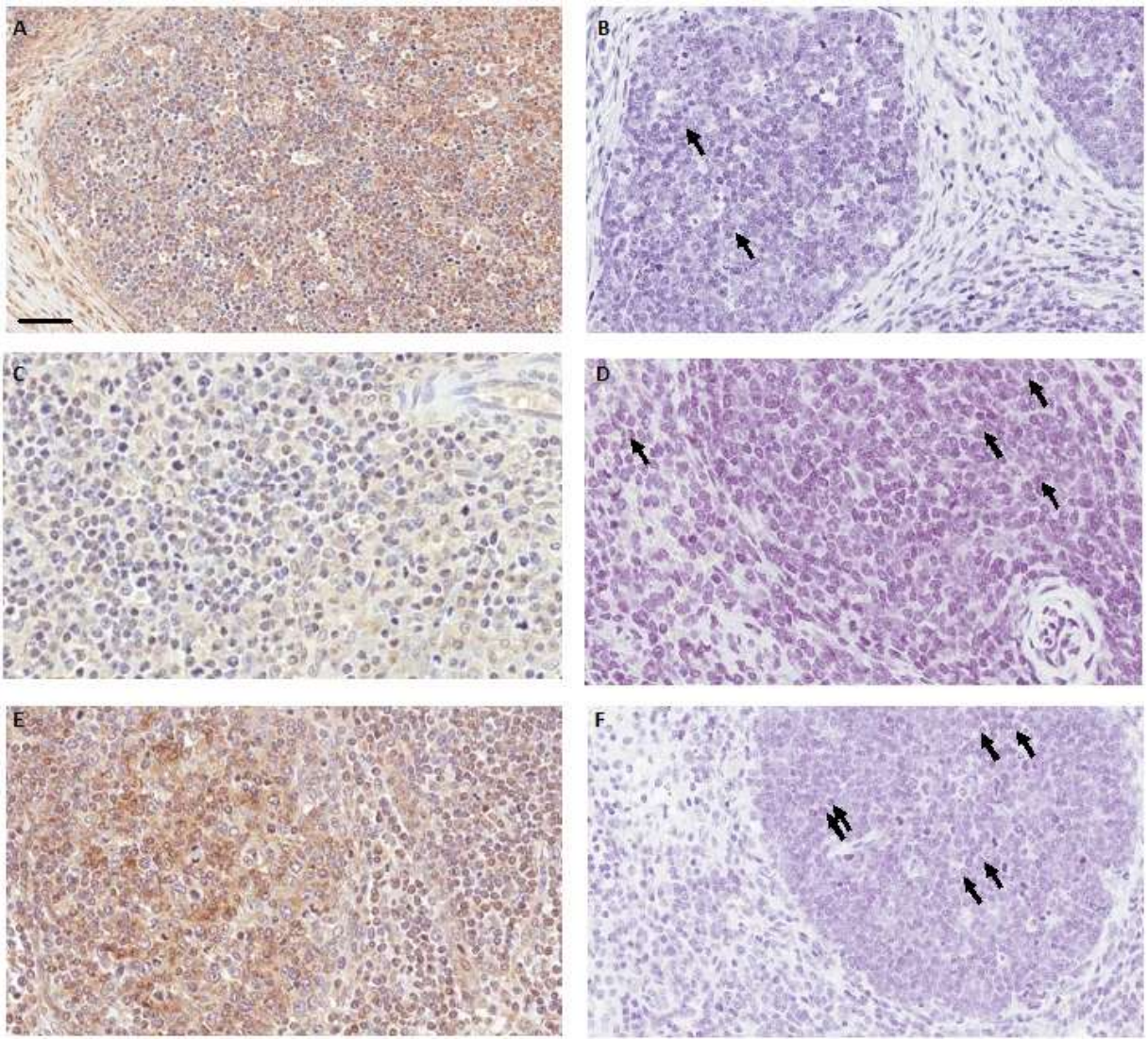

(A) TMPRSS2 signal in the gut associated lymphoid tissue (GALT) in the ileum. **(B)** Ileal GALT expression of *TMPRSS2* in cells morphologically consistent with lymphocytes (arrows). **(C)** TMPRSS2 expression in splenic white pulp. **(D)** *TMPRSS2* expression in leukocytes of the spleen (arrows). **(E)** Expression of TMPRSS2 in lymph node follicles. **(F)** *TMPRSS2* labeling in lymph node follicles (arrows). Bar is 50 μm and applies to all images.

Figure 14. TMPRSS2 and *TMPRSS2* expression in the tonsil

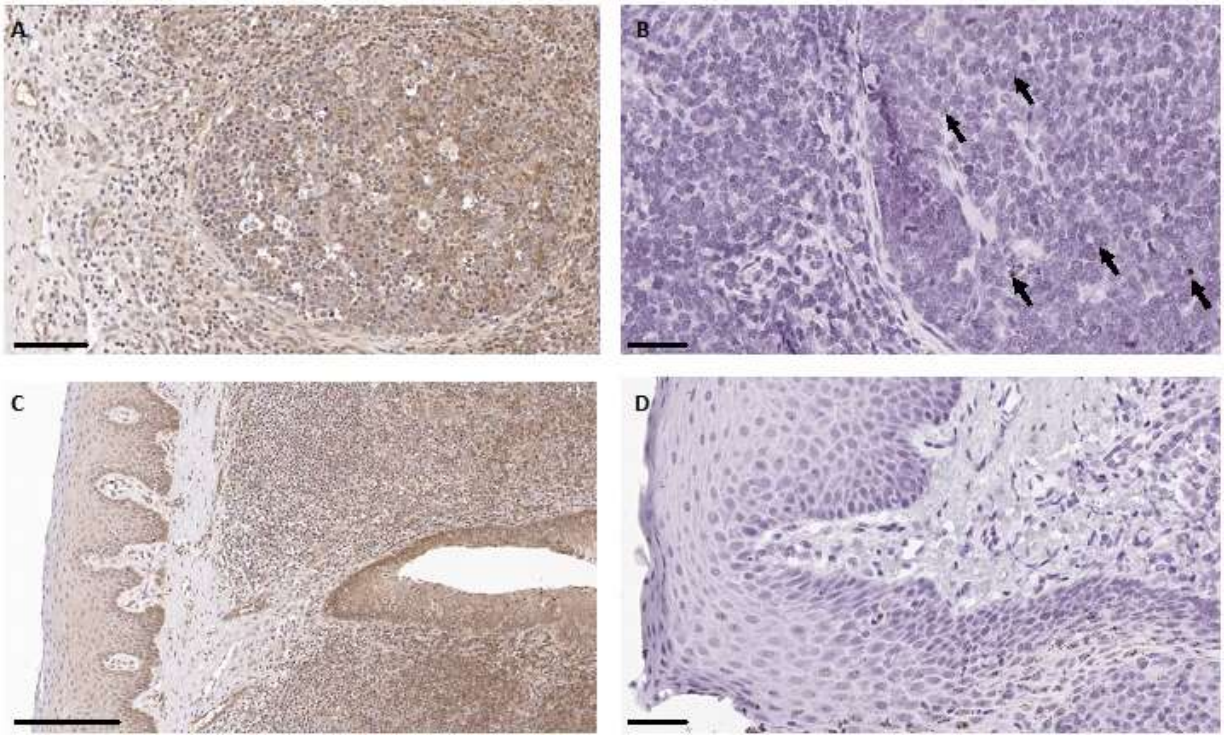

(A) Expression of TMPRSS2 in a tonsillar lymphoid follicle (bar is 100 μm) **(B)** Tonsillar follicular lymphocytes labeled for *TMPRSS2* (arrows) (bar is 50 μm). **(C)** TMPRSS2 labeling of the tonsillar epithelial layers and crypts (bar is 200 μm). **(D)** Expression of *TMPRSS2* in the epithelial layers and crypts (bar is 50 μm).

Table 6. TMPRSS2 and *TMPRSS2* expression patterns in additional tissues

Tissues	Structures	IHC	ISH
Liver	Hepatocytes	+	O+
	Kupffer	R+	R+
	Bile duct	+	+
	Vascular endothelium	+	R+
Spleen	PALS lymphocytes	O+	R+
	Lymphoid follicles	O+	O+
	Red pulp	-	R+
	Vascular endothelium	+	R+
Tonsil	Epithelium	+	O+
	Crypts	+	+
	Lymphoid follicles	O+	R+
Adrenal	Zona glomerulosa	+	R+
	Zona fasciculata	+	R+
	Zona reticularis	+	R+
	Ganglion cells	+	+
Pancreas	Vascular endothelium	+	-
	Acinar cells	+	O+
	Centeroacinar cells	+	+
	Islets of Langerhans	-	R+
	Extralobular duct	+	+
	Intralobular duct	+	+
Lymph node	Lymphoid follicles	O+	R+
	Lymphoid tissue	R+	R+
	Vascular endothelium	+	-
Skin	Epithelium	+	R+
	Dermal glands	+	+
	Dermal ducts	+	+
	Hair follicles	+	O+
Eye	Epithelium	N/A	N/A
Heart	Muscle cells	-	-
	Vascular endothelium	+	-

(+) = positive, (O+) = occasionally positive, (R+) = rarely positive,
(-) = negative, N/A = not available

Chapter 4 - Conclusion

To better understand mechanisms of diseases in humans and other animals, investigative (experimental) pathologists employ different animals as biomedical research models. While a diversity of animal species has been useful as experimental animal models in biomedical research, pigs could potentially be a better model due to the developmental and physiological similarities between them and humans. However, characterization of porcine immune responses to infectious diseases, such as influenza, is still limited [3]. Consequently, this body of work focused on (1) development of a set of lymphocyte markers for immunohistochemistry (IHC) as part of a larger study on naturally occurring severe combined immunodeficiency (SCID) in pigs and (2) determining the protein and mRNA expression patterns of type II transmembrane protease, serine S1 member 2 (TMPRSS2) in a diversity of porcine tissues and comparing these expression patterns to those reported in humans and mice.

First, we successfully developed IHC protocols for a previously unavailable set of T and B lymphocyte markers for formalin-fixed, paraffin-embedded (FFPE) tissue. While other techniques such as flow cytometry are available to evaluate immune cell populations, these techniques do not provide information on the cell type distribution within tissues. Consequently, this work provided IHC protocols for lymphocyte markers CD3, CD4, and Pax-5 for evaluation of the distribution and colocalization of T and B lymphocytes. In addition to their use in SCID pig characterization, the CD3 and Pax-5 duplex protocol will be immediately useful in the KS VDL for diagnostic and research cases. Additionally, we were able to develop a dual CD3/CD4 protocol to analyze the T helper cell distribution in relation to the total T lymphocyte population. Future directions for this research include validating an antibody for cytotoxic T lymphocytes

(CD8+) IHC and development of a duplex CD4/CD8 IHC to evaluate these mature T lymphocyte subsets in relation to each other.

Second, we characterized the mRNA and protein expression patterns of host cell protease, type II transmembrane protease, serine S1 member 2 (TMPRSS2), in over 30 FFPE porcine tissues. TMPRSS2's role in prostate cancer [58] and the observation that a TMPRSS2 knockout mouse has no phenotypic change or reproductive fitness issues [11, 38] led to a search for its role in other diseases. Further research revealed TMPRSS2's interaction with respiratory viruses, specifically influenza A virus. TMPRSS2 is expressed within the respiratory tract, gastrointestinal tract, urogenital tract, and various other organs in human and mouse tissues. However, TMPRSS2 has only been reported in a couple primary respiratory cell lines in the pig. Since pigs and humans are susceptible to many of the same strains of influenza, it is important to understand the expression of this protease in pigs and compare that to humans. Consequently, this work addressed a perceived need for broader characterization of this protease's expression in porcine tissues. Our results showed that pig expression patterns mimic the expression patterns in the human respiratory tract better than mouse expression patterns do. Hence the pig is a promising experimental animal model for further research into the role of TMPRSS2 in influenza pathogenesis and remains an interesting antiviral target. A unique benefit of using immunohistochemistry and *in situ* hybridization to evaluate TMPRSS2 expression is that both mRNA and protein can be reviewed at the tissue and cellular level, including identification of cell types which may secrete TMPRSS2 based on presence of antigen signal in the adjacent extracellular space. To our knowledge, this work provides the most detailed TMPRSS2 protein and mRNA expression profile available in any species and demonstrates the important similarities in TMPRSS2 expression in pigs and humans. These finding support the use of pigs as

an experimental animal model in influenza research as well as research of a variety of infectious diseases and cancers in which TMPRSS2 plays a role.

The overall goal of this thesis was to expand available knowledge on pigs as a model for biomedical research by focusing on the microscopic localization of lymphocyte cell markers and a protease of interest in formalin-fixed, paraffin-embedded (FFPE) porcine tissues. In future studies, these projects could come together in an examination of which lymphocyte subsets express TMPRSS2. Evaluation of which immune cells are expressing TMPRSS2 could lead to analysis of the potential role that these TMPRSS2 positive lymphocytes have in influenza infection. Research pertaining to TMPRSS2's role in other viral diseases, such as SARS and hepatitis C, could lead to novel antiviral treatments. In conclusion, this work provides tools to further characterize SCID pigs and new information about TMPRSS2 expression in pigs, both of value to the use of pigs in biomedical research.

References

1. Franco, N.H., *Animal Experiments in Biomedical Research: A Historical Perspective.* Animals : an open access journal from MDPI, 2013. **3**(1): p. 238-73.
2. Margine, I. and F. Krammer, *Animal models for influenza viruses: implications for universal vaccine development.* Pathogens (Basel, Switzerland), 2014. **3**(4): p. 845-74.
3. DS, R. and V. AL, - *Swine as a model for influenza A virus infection and immunity.* Ilar J, 2015. **56**(1): p. 44-52.
4. Waide, E.H., et al., *Not All SCID Pigs Are Created Equally: Two Independent Mutations in the Artemis.* J Immunol, 2015. **195**(7): p. 3171-9.
5. S, B., et al., *TMPRSS2 and TMPRSS4 facilitate trypsin-independent spread of influenza virus in.* J Virol, 2010. **84**(19): p. 10016-25.
6. Bertram, S., et al., *Influenza and SARS-Coronavirus Activating Proteases TMPRSS2 and HAT Are Expressed at Multiple Sites in Human Respiratory and Gastrointestinal Tracts (Proteolytic Activation of Influenza and SARS).* PLoS ONE, 2012. **7**(4): art. no. e35876.
7. E, B.-F., et al., *Inhibition of influenza virus infection in human airway cell cultures by an antisense peptide-conjugated morpholino oligomer targeting the hemagglutinin-activating protease TMPRSS2. .* J Virol, 2011. **85**(4): p. 1554-62.
8. Donaldson, S.H., et al., *Regulation of the epithelial sodium channel by serine proteases in human airways.* The Journal of biological chemistry, 2002. **277**(10): p. 8338-45.
9. Vaarala, M.H., et al., *Expression of transmembrane serine protease TMPRSS2 in mouse and human tissues.* Journal of Pathology, 2001. **193**(1): p. 134-140.
10. Iwata-Yoshikawa, N., et al., *TMPRSS2 Contributes to Virus Spread and Immunopathology in the Airways of Murine Models after Coronavirus Infection.* Journal of virology, 2019. **93**(6). p. 1815-18
11. Kim, T.S., et al., *Phenotypic analysis of mice lacking the Tmprss2-encoded protease.* Molecular and cellular biology, 2006. **26**(3): p. 965-75.
12. Böttcher-Friebertshäuser, E., H.D. Klenk, and W. Garten, *Activation of influenza viruses by proteases from host cells and bacteria in the human airway epithelium*. PAthogens and Disease, 2013. p. 87-100.
13. Charerntantanakul, W. and J.A. Roth, *Biology of porcine T lymphocytes.* Anim. Health. Res. Rev., 2006. **7**(1-2): p. 81-96.
14. Mestas, J. and C.C. Hughes, *Of mice and not men: differences between mouse and human immunology.* J Immunol, 2004. **172**(5): p. 2731-8.
15. EM, W. and P. RS, - *Advancing swine models for human health and diseases.* Mo Med, 2013. **110**(3): p. 212-5.
16. AG, O., et al., - *Preliminary findings of a previously unrecognized porcine primary.* Vet Pathol, 2013. **50**(1): p. 144-6.
17. Ramos-Vara, J.A., *Technical aspects of immunohistochemistry.* Vet Pathol, 2005. **42**(4): p. 405-26.
18. JA, R.-V., et al., - *Suggested guidelines for immunohistochemical techniques in veterinary diagnostic.* J Vet Diagn Invest, 2008. **20**(4): p. 393-413.
19. L, P.-G. and S. H, - *Membrane markers of the immune cells in swine: an update.* Vet Res, 2008. **39**(6): p. 39-54.

20. Elmore, S.A., *Enhanced Histopathology of the Spleen.* Toxicologic Pathology, 2006. **34**(5): p. 648-655.
21. Bianchi, A.T.J., et al., *Development of the B- and T-cell compartments in porcine lymphoid organs from birth to adult life: an immunohistological approach.* Veterinary Immunology and Immunopathology, 1992. **33**(3): p. 201-221.
22. Desouki, M.M., et al., *PAX-5: a valuable immunohistochemical marker in the differential diagnosis of lymphoid neoplasms.* Clinical medicine & research, 2010. **8**(2): p. 84-88.
23. Banks, W.J., *Applied veterinary histology*. 3rd edition.. ed. 1993, St. Louis, Mo.: St. Louis, Mo. : Mosby Year Book. p. 75-82.
24. Randall, K.J. and G. Pearse, *A Dual-label Technique for the Immunohistochemical Demonstration of T-Lymphocyte Subsets in Formalin-Fixed, Paraffin-Embedded Rat Lymphoid Tissue.* Toxicologic Pathology, 2008. **36**(6): p. 795-804.
25. Zuckermann, F.A. and H.R. Gaskins, *Distribution of porcine CD4/CD8 double-positive T lymphocytes in mucosa-associated lymphoid tissues.* Immunology, 1996. **87**(3): p. 493-499.
26. Hooper, J.D., et al., *Type II transmembrane serine proteases. Insights into an emerging class of cell surface proteolytic enzymes.* The Journal of biological chemistry, 2001. **276**(2): p. 857-860.
27. Szabo, R. and T.H. Bugge, *Type II transmembrane serine proteases in development and disease.* International Journal of Biochemistry and Cell Biology, 2008. **40**(6): p. 1297-1316.
28. Netzel-Arnett, S., et al., *Membrane anchored serine proteases: A rapidly expanding group of cell surface proteolytic enzymes with potential roles in cancer.* Cancer and Metastasis Reviews, 2003. **22**(2): p. 237-258.
29. Choi, S.-Y., et al., *Type II transmembrane serine proteases in cancer and viral infections.* Trends in Molecular Medicine, 2009. **15**(7): p. 303-312.
30. Böttcher, E., et al., *Proteolytic activation of influenza viruses by serine proteases TMPRSS2 and HAT from human airway epithelium.* Journal of virology, 2006. **80**(19): p. 9896-8.
31. E, B., et al., - *MDCK cells that express proteases TMPRSS2 and HAT provide a cell system to.* Vaccine, 2009. **27**(45): p. 6324-9.
32. S, B., et al., - *Influenza and SARS-coronavirus activating proteases TMPRSS2 and HAT are expressed.* PLoS One, 2012. **7**(4): art. no. e35876 .
33. B, H., et al., - *Tmprss2 is essential for influenza H1N1 virus pathogenesis in mice.* PLoS Pathog, 2013. **9**(12). art. no. e1003774 , p. 1-10.
34. NM, B. and P. P, - *The biology of influenza viruses.* Vaccine, 2008. **12**(26): p. D49-53.
35. Kido, H., et al., *Proteases essential for human influenza virus entry into cells and their inhibitors as potential therapeutic agents.* Current pharmaceutical design, 2007. **13**(4): p. 405-14.
36. S, B., et al., - *TMPRSS2 and TMPRSS4 facilitate trypsin-independent spread of influenza virus in.* J Virol, 2010. **84**(19): p. 10016-25.
37. Sakai, K., et al., *The host protease TMPRSS2 plays a major role in in vivo replication of emerging H7N9 and seasonal influenza viruses.* Journal of virology, 2014. **88**(10): p. 5608-16.

38. Tarnow, C., et al., *TMPRSS2 is a host factor that is essential for pneumotropism and pathogenicity of H7N9 influenza A virus in mice.* Journal of virology, 2014. **88**(9): p. 4744-51.
39. World Health, Organization. *Human infection with avian influenza A(H7N9) virus – China: Update* 2018; Available from: https://www.who.int/csr/don/05-september-2018-ah7n9-china/en/.
40. Bouvier, N.M. and A.C. Lowen, *Animal Models for Influenza Virus Pathogenesis and Transmission.* Viruses, 2010. **2**(8): p. 1530-63.
41. Peitsch, C., et al., *Activation of influenza A viruses by host proteases from swine airway epithelium.* Journal of virology, 2014. **88**(1): p. 282-291.
42. C, P., et al., - *Activation of influenza A viruses by host proteases from swine airway epithelium.* J Virol, 2014. **88**(1): p. 282-291.
43. Whitworth, K., et al., *Zygote injection of CRISPR/Cas9 RNA successfully modifies the target gene without delaying blastocyst development or altering the sex ratio in pigs.* Associated with the International Society for Transgenic Technologies (ISTT), 2017. **26**(1): p. 97-107.
44. Shi, W., et al., *TMPRSS2 and MSPL Facilitate Trypsin-Independent Porcine Epidemic Diarrhea Virus Replication in Vero Cells.* Viruses, 2017. **9**(5): p. 114-131.
45. Bugge, T.H., T.M. Antalis, and Q. Wu, *Type II transmembrane serine proteases.* The Journal of biological chemistry, 2009. **284**(35): p. 23177-23181.
46. MH, V., et al., - *Expression of transmembrane serine protease TMPRSS2 in mouse and human tissues.* J Pathol, 2001. **193**(1): p. 134-40.
47. Ibricevic, A., et al., *Influenza virus receptor specificity and cell tropism in mouse and human airway epithelial cells.* Journal of virology, 2006. **80**(15): p. 7469-80.
48. Van Poucke, S., et al., *Replication of avian, human and swine influenza viruses in porcine respiratory explants and association with sialic acid distribution.* Virology journal, 2010. **7**(1). p.7-38.
49. M, A., et al., - *TMPRSS2 is an activating protease for respiratory parainfluenza viruses.* J Virol, 2013. **87**(21): p. 11930-11935.
50. Shirogane, Y., et al., *Efficient multiplication of human metapneumovirus in Vero cells expressing the transmembrane serine protease TMPRSS2.* Journal of virology, 2008. **82**(17): p. 8942-46.
51. Abe, M., et al., *TMPRSS2 is an activating protease for respiratory parainfluenza viruses.* Journal of virology, 2013. **87**(21): p. 11930-35.
52. Matsuyama, S., et al., *Efficient activation of the severe acute respiratory syndrome coronavirus spike protein by the transmembrane protease TMPRSS2.* Journal of virology, 2010. **84**(24): p. 12658-12664.
53. S, B., et al., - *TMPRSS2 activates the human coronavirus 229E for cathepsin-independent host cell.* J Virol, 2013. **87**(11): p. 6150-6160.
54. Chen, W., et al., *SARS-associated coronavirus transmitted from human to pig.* Emerging Infectious Diseases, 2005. **11**(3): p. 446-448.
55. Esumi, M., et al., *Transmembrane serine protease TMPRSS2 activates hepatitis C virus infection.* Hepatology, 2015. **61**(2): p. 437-446.
56. Jacquinet, E., et al., *Cloning and characterization of the cDNA and gene for human epitheliasin.* European Journal of Biochemistry, 2001. **268**(9): p. 2687-2699.

57. Govorkova, E.A. and R.G. Webster, *Combination Chemotherapy for Influenza.* Viruses, 2010. **2**(8): p. 1510-1529.
58. E, P.-G., et al., - *In vitro characterization of TMPRSS2 inhibition in IPEC-J2 cells.* J Enzyme Inhib Med Chem, 2016. **31**(sup2): p. 123-129.